
Language-Critique Imitation Learning from Suboptimal Demonstrations

Chih-Han Yang¹ Dai-Jie Wu^{2*} Yun-Ping Huang^{1*} Ping-Chun Hsieh³
Kenneth Marino² Shao-Hua Sun^{1,4}

¹Graduate Institute of Communication Engineering, National Taiwan University (NTU)

²University of Utah

³National Yang Ming Chiao Tung University

⁴NTU Artificial Intelligence Center of Research Excellence

Abstract

Prior work on imitation learning from suboptimal demonstrations typically relies on compressed supervision signals such as confidence estimates, discriminator scores, or importance weights. These scalar signals are inherently limited, as they cannot explicitly express intermediate reasoning about task progress, failure modes, or corrective actions. We propose a language-critique framework for imitation learning from suboptimal demonstrations that instead leverages natural language as a structured supervision signal, avoiding the collapse of expressive feedback into scalars. Our method first constructs language labels from demonstrations that explicitly describe current progress, identify suboptimal behaviors, and provide fine-grained corrective guidance. We then introduce a language-critique loss that directly trains policies using these structured signals without reducing them to scalars, and instantiate it for both behavior cloning and diffusion policies, yielding LC-BC and LC-DP. We further provide a theoretical result showing that the proposed objective upper-bounds the expert performance gap under standard assumptions. Empirically, we evaluate on diverse continuous control tasks spanning navigation, manipulation, and gameplay, where our methods consistently outperform strong imitation learning and offline reinforcement learning baselines. These results demonstrate that language can serve as a powerful and structured form of supervision for learning robust policies from suboptimal data.

1 Introduction

Imitation learning (IL; [1–5]) has achieved strong results in navigation, driving, robotic control, game playing, and embodied decision making, but policies trained on limited demonstrations often suffer from compounding error [6] and distribution shift [7]. A natural remedy is to collect more expert data, yet expert demonstrations are costly and often difficult to scale [8]. Online imitation methods, such as adversarial and distribution-matching approaches [9–14], can reduce this gap by querying the environment or an expert during training, but such interaction is often unsafe, expensive, or impractical in real-world settings. This has motivated imitation learning from suboptimal demonstrations [15–25], where a small amount of expert data is supplemented with abundant imperfect trajectories that are cheaper and easier to collect. When properly exploited, these suboptimal demonstrations can improve state-action coverage and policy robustness without requiring additional environment interaction.

The key challenge is how to extract useful supervision from mixed-quality offline data. Existing methods typically reduce supervision to scalar signals such as confidence estimates [19, 24], discriminator scores [20–23], importance weights [15–18], or rewards (*i.e.*, offline RL [26–30]). While these

*Equal contribution

scalar signals can rank trajectories, they remain highly compressed: they say little about what went wrong, what subgoal should come next, or how behavior should be corrected. As a result, they often fail to capture the structured information that is present in demonstrations, especially in long-horizon or multimodal tasks where progress depends on subtle decisions and stage-specific corrections.

Natural language offers a richer alternative. Instead of collapsing behavior into a single score, language can describe task progress, subgoals, action quality, failure modes, and corrective guidance [31–37]. For example, in a multi-stage manipulation task (BLOCKPUSH in Figure 3d) where a robot arm must push two blocks into target regions, language labels can indicate which object to approach, which target to prioritize, and how to adjust the motion, rather than merely assigning a higher or lower reward. This makes language particularly attractive as a supervision signal for learning from suboptimal demonstrations. However, two challenges remain: (1) language labels are not naturally available in offline continuous control datasets, and (2) existing methods often convert language back into scalar rewards or preferences, discarding much of its descriptive power [38–41].

To address these challenges, we introduce language-critique imitation learning from suboptimal demonstrations, an offline IL framework that adds language guidance to learning from expert and suboptimal demonstrations and explicitly uses that guidance to train policies. Our method first constructs structured language labels that describe task progress, action optimality, and movement guidance from offline trajectories. We then design a language-critique loss that uses these labels directly to supervise policy learning, without reducing them to scalar rewards or weights. This loss is applied to both behavior cloning [1] and diffusion policies [42], yielding language-critique behavior cloning (LC-BC) and language-critique diffusion policy (LC-DP) as end-to-end offline learning algorithms. We also provide a theoretical justification showing that the proposed language-critique loss upper-bounds the expert-policy performance gap under standard assumptions [43, 44].

We evaluate our framework on eight diverse continuous-control tasks spanning navigation, gameplay, and manipulation, including multimodal and precision-manipulation settings. Across these tasks, the proposed language-guided methods, LC-BC and LC-DP, consistently outperform prior imitation learning approaches (*e.g.*, DemoDICE [17], DWBC [20]) and offline RL methods (*e.g.*, CQL [27], DT [28], TD3+BC [29]), with especially large gains in multimodal, long-horizon, and precision-control settings. Ablation studies further show that both the structured language design and the language-critique loss are essential, and that the method remains effective even when the expert partition is imperfect. Together, these results show that language is not merely a descriptive aid: it is a powerful supervision signal for learning from suboptimal demonstrations.

2 Related works

Imitation learning (IL) enables agents to mimic behaviors from expert demonstrations [2, 45]. Online IL methods [7, 9, 10] improve robustness through online environment interaction and expert correction, which incurs high costs and may involve unsafe interactions during training. Offline IL methods based on behavioral cloning [1, 15] instead learn from static datasets, avoiding additional interaction but often suffering from compounding errors [6] and distribution shift [7]. To address these limitations, recent work augments limited expert data with abundant suboptimal demonstrations [16, 23, 24, 46], leveraging techniques such as discriminator- or confidence-based reweighting and behavior purification [17–22, 47]. Complementary approaches formulate offline IL as inverse reinforcement learning, recovering rewards or world models from mixed-quality data [48–51]. More recently, diffusion policies have further improved robustness and multimodal behavior modeling [42, 52–54]. Our method follows this offline IL setting with expert and suboptimal demonstrations, while further incorporating language label supervision directly from offline data.

Offline reinforcement learning (offline RL) [26, 55] learns policies from static datasets without additional environment interaction, but suffers from distribution shift, out-of-distribution actions, and value overestimation. Existing methods address these issues through conservative or implicit value learning [27, 56], uncertainty estimation [57], value-guided behavior cloning [58], and conservative model-based planning [59, 60]. More recently, generative approaches formulate offline RL as sequence modeling [28] or parameterize policies with expressive models such as VAEs and diffusion policies [30, 61–63], including Q-guided diffusion and diffusion-based planning [64–67]. However, these methods ultimately rely on scalar reward supervision, whereas our approach instead leverages more expressive language label supervision for offline policy learning.

Learning from language. Natural language has been widely used in decision-making and control, primarily as task instructions or conditioning signals for improving generalization [68–74, 37]. However, most existing methods focus on discrete or text-based domains, with limited study in continuous control [75–78]. Other approaches convert language into scalar rewards or preferences [38–41, 79], losing much of its structural information. In contrast, our work uses language labels as direct supervision for offline policy learning, preserving the expressiveness of language to enable robust learning from suboptimal demonstrations.

3 Preliminaries

Markov decision process. A finite-horizon Markov decision process (MDP) is defined by the tuple $\mathcal{M} := (\mathcal{S}, \mathcal{A}, P, r, \rho_0, \gamma, T)$, where \mathcal{S} and \mathcal{A} are the state and action spaces, $P(s' | s, a)$ is the transition function, $r : \mathcal{S} \times \mathcal{A} \rightarrow \mathbb{R}$ is the reward function, ρ_0 is the initial state distribution, $\gamma \in (0, 1)$ is the discount factor, and T is the horizon. A policy $\pi : \mathcal{S} \rightarrow \Delta(\mathcal{A})$ induces a trajectory distribution with $s_0 \sim \rho_0$, and we denote the expected discounted return by $J_r(\pi) := \mathbb{E}_{\tau \sim \pi} \left[\sum_{t=0}^{T-1} \gamma^t r(s_t, a_t) \right]$.

Offline imitation learning from suboptimal demonstrations. We consider offline imitation learning with an expert dataset $\mathcal{D}_E = \{\tau_i^E\}_{i=1}^M$ of M trajectories from expert policy π_E , where $\tau_i^E = \{(s_{i,t}, a_{i,t}^E)\}_{t=0}^{|\tau_i^E|-1}$. The learner also has access to a general dataset $\mathcal{D}_G = \{\tau_i^\beta\}_{i=1}^N$ of N state-action trajectories $\tau_i^\beta = \{(s_{i,t}, a_{i,t})\}_{t=0}^{|\tau_i^\beta|-1}$ collected by behavior policies π_β [26, 80], spanning expert-like, suboptimal, and random behaviors, with $\mathcal{D}_E \subset \mathcal{D}_G$. The goal is to learn a policy π_θ that imitates expert behavior while exploiting useful behaviors in \mathcal{D}_G . This motivates supervision signals that identify useful behaviors in heterogeneous offline data. Additional details are in Section F.

4 Approach

We present language-critique imitation learning from suboptimal demonstrations, an offline framework that supervises policy learning with structured language labels instead of scalar signals. Section 4.1 formulates the language-critique objective and performance guarantee, Section 4.2 instantiates a structured language label generator μ_g , and Section 4.3 distills μ_g into a differentiable LLM-Captioner μ_ϕ with the language-critique loss to train BC and diffusion policies.

4.1 From action imitation to language-critique imitation

We use language labels to describe state-action features, distinguish expert from suboptimal behaviors, and exploit them through our language-critique imitation objective. Let μ denote a language label function conditioned on a state-action pair. For expert state $s_t \sim d_{\pi_E}^t$, action $a_t^E \sim \pi_E(\cdot | s_t)$, and label $l_t^E \sim \mu(\cdot | s_t, a_t^E)$, we score a policy action $\hat{a}_t \sim \pi_\theta(\cdot | s_t)$ by the likelihood it assigns to l_t^E :

$$J_{\text{LC}}(\pi_\theta) := \sum_{t=0}^{T-1} \gamma^t \mathbb{E}_{s_t \sim d_{\pi_E}^t, a_t^E \sim \pi_E(\cdot | s_t), l_t^E \sim \mu(\cdot | s_t, a_t^E), \hat{a}_t \sim \pi_\theta(\cdot | s_t)} [\log \mu(l_t^E | s_t, \hat{a}_t)]. \quad (1)$$

Mirroring the performance difference formulation in Lemma A.1, we define the language-critique gap as $\Delta_{\text{LC}}(\pi_\theta) := J_{\text{LC}}(\pi_E) - J_{\text{LC}}(\pi_\theta)$. Since $J_{\text{LC}}(\pi_E)$ is independent of π_θ , minimizing $\Delta_{\text{LC}}(\pi_\theta)$ is equivalent to maximizing $J_{\text{LC}}(\pi_\theta)$. Expanding the gap gives

$$\Delta_{\text{LC}}(\pi_\theta) = \sum_{t=0}^{T-1} \gamma^t \mathbb{E}_{s_t \sim d_{\pi_E}^t, a_t^E \sim \pi_E(\cdot | s_t), l_t^E \sim \mu, \hat{a}_t \sim \pi_\theta(\cdot | s_t)} [\log \mu(l_t^E | s_t, a_t^E) - \log \mu(l_t^E | s_t, \hat{a}_t)]. \quad (2)$$

Intuitively, the gap penalizes policy actions that make the expert critique less likely than the expert action. In Section A, we show that under standard linear-feature realizability and a **language-sufficiency condition** on μ , minimizing $\Delta_{\text{LC}}(\pi_\theta)$ controls the expert-state performance gap and recovers expert behavior. The condition rules out uninformative labels and requires μ to preserve distinctions in state-action features $\psi(s, a) : \mathcal{S} \times \mathcal{A} \rightarrow \mathbb{R}^d$: if two actions a, a' at the same state differ, $\mu(\cdot | s, a)$ and $\mu(\cdot | s, a')$ should be distinguishable. We realize this principle with a structured generator μ_g (Section 4.2) and differentiable distillation μ_ϕ for policy optimization (Section 4.3).

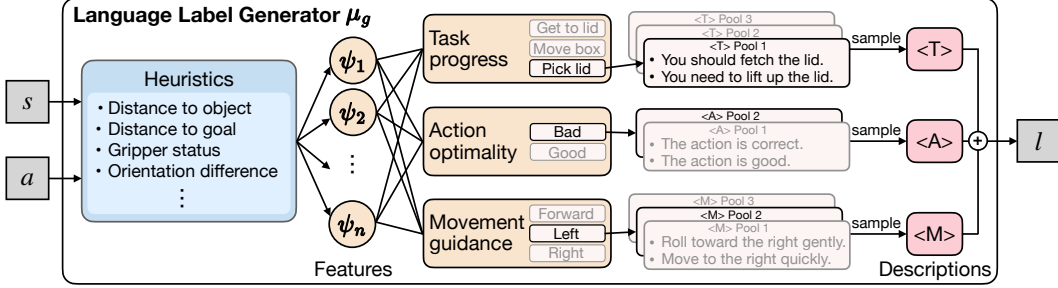


Figure 1: **Language label generator** μ_g . Given a state-action pair (s, a) , μ_g extracts task-specific features (e.g., object distance, gripper status) and routes them to three selectors: task progress $\langle T \rangle$, action optimality $\langle A \rangle$, and movement guidance $\langle M \rangle$. Each selector samples a description snippet, concatenated into the final language label l for scalable and structured supervision.

4.2 Language label generation

To satisfy the language-critique sufficiency in Section 4.1, we define a structured generator μ_g over state-action pairs. Compared with other μ candidates (e.g., human or free-form LLM/VLM annotations), this design is cheaper, more consistent, and less prone to prompt sensitivity and control-irrelevant variation.

Motivated by reward design principles [81, 82], each label has three components: task progress $\langle T \rangle$, action optimality $\langle A \rangle$, and movement guidance $\langle M \rangle$. They capture the current stage, whether an action is desirable, and how it should be corrected, while suppressing irrelevant linguistic variation. As shown in Figure 1 and detailed in Section C, μ_g extracts task-relevant heuristics (e.g., object distance and gripper status) from a state-action pair (s_t, a_t) without privileged environmental information, and routes them to three component-specific selectors, each sampling a snippet from a pool. Concatenating the snippets yields the final language label l_t . Applying μ_g to each state-action pair in \mathcal{D}_E and \mathcal{D}_G gives language-labeled datasets, where l_t denotes the generated language label for (s_t, a_t) :

$$\mathcal{D}_E^{\text{lang}} = \{(s_t, a_t^E, l_t^E) \mid (s_t, a_t^E) \in \mathcal{D}_E, l_t^E \sim \mu_g(\cdot \mid s_t, a_t^E)\}, \quad (3)$$

$$\mathcal{D}_G^{\text{lang}} = \{(s_t, a_t, l_t) \mid (s_t, a_t) \in \mathcal{D}_G, l_t \sim \mu_g(\cdot \mid s_t, a_t)\}. \quad (4)$$

4.3 Language-critique imitation learning

To enable end-to-end policy optimization, we instantiate the theoretical gap $\Delta_{\text{LC}}(\pi_\theta)$ with \mathcal{L}_{LC} , a token-level cross-entropy loss computed through the differentiable language label function μ_ϕ , namely the LLM-Captioner. The full method is illustrated in Figure 2.

LLM-Captioner. We distill the language label generator μ_g into a differentiable LLM-Captioner μ_ϕ that maps state-action pairs to structured language label outputs. Because μ_ϕ is differentiable, gradients from the language objective in Equation (2) can back-propagate to π_θ , enabling joint optimization instead of a staged pipeline that collapses language to scalar targets. Architecturally, μ_ϕ bridges continuous control and language labels by combining a pretrained LLM with an MLP projector that maps state-action pairs into the transformer’s hidden space; details appear in Section D and I.2. We fine-tune μ_ϕ on $\mathcal{D}_G^{\text{lang}}$ with token-level cross entropy:

$$\ell_{\text{CE}}^\phi(l_t, s_t, a_t) = -\frac{1}{N_t} \sum_{n=1}^{N_t} \log \mu_\phi(l_{t,n} \mid l_{t,<n}, s_t, a_t) \quad (5)$$

where N_t denotes the tokenized sequence length of l_t . Both the LLM-backbone and the projector are updated according to this objective:

$$\mathcal{L}_{\text{CE}} = \mathbb{E}_{(s_t, a_t, l_t) \sim \mathcal{D}_G^{\text{lang}}} \left[\ell_{\text{CE}}^\phi(l_t, s_t, a_t) \right] \quad (6)$$

After fine-tuning, we freeze μ_ϕ and use it for downstream policy optimization. Since the general dataset contains both expert and suboptimal demonstrations, μ_ϕ learns a discriminative mapping from

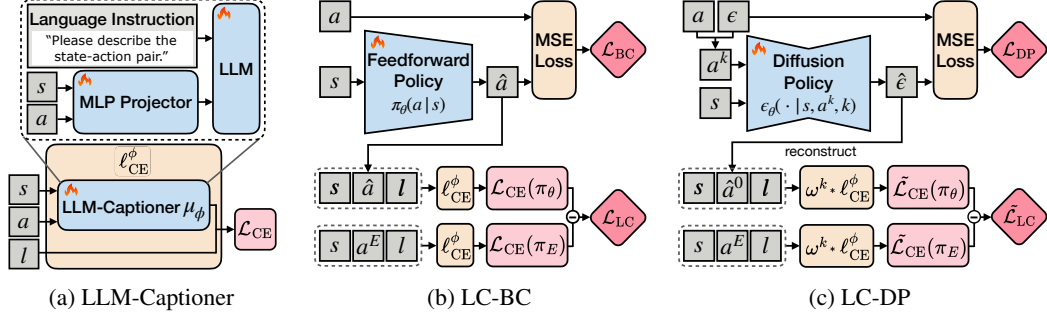


Figure 2: **(a) LLM-Captioner architecture and fine-tuning.** LLM-Captioner uses an LLM backbone and MLP projector to map state-action pairs into the transformer’s hidden space. We fine-tune μ_ϕ on $\mathcal{D}_G^{\text{lang}}$ to distill μ_ϕ . **(b) Language-critique behavior cloning (LC-BC).** A feedforward policy π_θ is trained with \mathcal{L}_{BC} and LC-loss \mathcal{L}_{LC} . The LC-loss applies cross-entropy ℓ_{CE}^ϕ to policy and expert actions via a frozen LLM-Captioner. **(c) Language-critique diffusion policy (LC-DP).** A diffusion policy ϵ_θ is trained with \mathcal{L}_{DP} and reweighted \mathcal{L}_{LC} . A step-dependent reweighting factor ω^k handles varying diffusion steps, and LC-loss applies to clean actions \hat{a}^0 reconstructed from predicted noise $\hat{\epsilon}$.

state-action pairs to language. Each component of the predicted language label exposes behavior-quality discrepancies, providing structured supervision that can be exploited during policy learning.

Language-critique loss. We then instantiate the practical language-critique loss through μ_ϕ . For a policy action $\hat{a}_t \sim \pi_\theta(\cdot | s_t)$ and expert action a_t^E , we define

$$\mathcal{L}_{CE}(\pi_\theta) = \mathbb{E}_{(s_t, l_t) \sim \mathcal{D}_E^{\text{lang}}, \hat{a}_t \sim \pi_\theta} \left[\ell_{CE}^\phi(l_t, s_t, \hat{a}_t) \right]. \quad (7)$$

$$\mathcal{L}_{CE}(\pi_E) = \mathbb{E}_{(s_t, a_t^E, l_t) \sim \mathcal{D}_E^{\text{lang}}} \left[\ell_{CE}^\phi(l_t, s_t, a_t^E) \right]. \quad (8)$$

The LC-loss clips the policy loss at the expert loss:

$$\mathcal{L}_{LC}(\pi_\theta, \pi_E) = [\mathcal{L}_{CE}(\pi_\theta) - \text{sg}(\mathcal{L}_{CE}(\pi_E))]_+, \quad (9)$$

where $[x]_+ = \max(x, 0)$ and $\text{sg}(\cdot)$ denotes stop-gradient. This loss is a differentiable surrogate for $\Delta_{LC}(\pi_\theta)$: it penalizes policy actions that make the expert language label less likely than the corresponding expert actions, and vanishes once the policy matches the expert under μ_ϕ . Each update transfers the behavior-quality distinctions learned by μ_ϕ from both expert and suboptimal data into the policy. In Section A.5, we show that \mathcal{L}_{LC} upper-bounds the performance gap between π_θ and π_E up to the captioner distillation residual, extending Theorem A.4 to the practical objective.

Language-critique imitation learning. We apply the LC-loss to behavior cloning (BC) and diffusion policy (DP) [42]. Training uses the expert-labeled dataset $\mathcal{D}_E^{\text{lang}}$, while the LC-loss transfers the behavior distinctions learned by μ_ϕ from the broader labeled dataset $\mathcal{D}_G^{\text{lang}}$, utilizing suboptimal demonstrations into auxiliary supervision. The LLM-Captioner is used only during training and incurs no test-time cost. First, for BC, a feedforward MLP policy π_θ is updated with

$$\mathcal{L}_{BC} = \mathbb{E}_{(s_t, a_t^E) \sim \mathcal{D}_E, \hat{a}_t \sim \pi_\theta} \left[\|a_t^E - \hat{a}_t\|_2^2 \right]. \quad (10)$$

Language-Critique Behavior Cloning (LC-BC) optimizes Equation (10) with the LC-loss: $\mathcal{L}_{BC} + \lambda \mathcal{L}_{LC}$, where λ controls LC-loss strength. For DP, the policy ϵ_θ is a UNet [83] noise-prediction model, yielding Language-Critique Diffusion Policy (LC-DP). Its standard objective is

$$\mathcal{L}_{DP} = \mathbb{E}_{(s_t, a_t^E) \sim \mathcal{D}_E, \epsilon \sim \mathcal{N}(0, \mathbf{I}), k} \left[\|\epsilon - \hat{\epsilon}\|_2^2 \right] \quad (11)$$

with $\hat{\epsilon} \sim \epsilon_\theta(\cdot | s_t, a_t^k, k)$ and $a_t^k = \sqrt{\bar{\alpha}^k} a_t^E + \sqrt{1 - \bar{\alpha}^k} \epsilon$. Since DP predicts noise rather than actions, we apply the LC-loss to one-step reconstructed action \hat{a}_t^0 from the sample a_t^k at diffusion step k :

$$\hat{a}_t^0 = \frac{1}{\sqrt{\bar{\alpha}^k}} a_t^k - \frac{\sqrt{1 - \bar{\alpha}^k}}{\sqrt{\bar{\alpha}^k}} \hat{\epsilon}, \quad \hat{\epsilon} \sim \epsilon_\theta(\cdot | s_t, a_t^k, k). \quad (12)$$

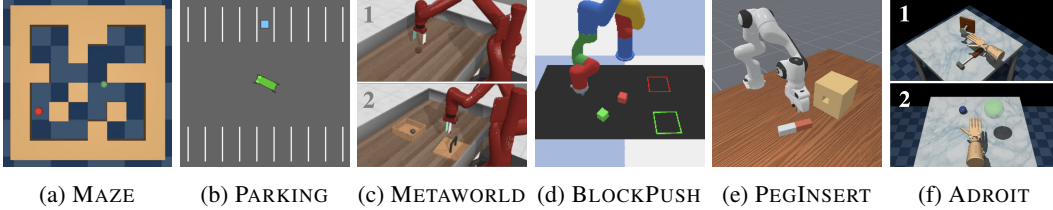


Figure 3: **Environments & tasks.** (a) **MAZE**: Navigate a green agent to a red goal. (b) **PARKING**: Park a green car in the blue spot. (c-1) **SWEEP**: Sweep a block sideways. (c-2) **BOX-CLOSE**: Place a lid onto a box. (d) **BLOCKPUSH**: Multi-stage multimodal task pushing two blocks to their targets. (e) **PEGINSERT**: Precisely insert a peg into a side hole. (f-1) **HAMMER**: High-dimensional control to hammer a nail. (f-2) **RELOCATE**: High-dimensional control to relocate a ball.

Since reconstructions from larger k are noisier, we weight each diffusion-step samples by $\omega^k = \frac{\bar{\alpha}^k}{1-\bar{\alpha}^k}$ and define the reweighted LC-loss as

$$\tilde{\mathcal{L}}_{\text{CE}}(\pi_\theta) = \mathbb{E}_{(s_t, l_t) \sim \mathcal{D}_E^{\text{lang}}, \hat{a}_t^0 \sim \epsilon_\theta(s_t), k} \left[\omega^k \ell_{\text{CE}}^\phi(l_t, s_t, \hat{a}_t^0) \right] \quad (13)$$

$$\tilde{\mathcal{L}}_{\text{CE}}(\pi_E) = \mathbb{E}_{(s_t, a_t^E, l_t) \sim \mathcal{D}_E^{\text{lang}}, k} \left[\omega^k \ell_{\text{CE}}^\phi(l_t, s_t, a_t^E) \right] \quad (14)$$

$$\tilde{\mathcal{L}}_{\text{LC}}(\pi_\theta, \pi_E) = \left[\tilde{\mathcal{L}}_{\text{CE}}(\pi_\theta) - \text{sg}(\tilde{\mathcal{L}}_{\text{CE}}(\pi_E)) \right]_+ \quad (15)$$

The LC-DP objective, $\mathcal{L}_{\text{DP}} + \lambda \tilde{\mathcal{L}}_{\text{LC}}$, encourages reconstructed actions to stay close to expert actions while inducing expert-consistent language labels under μ_ϕ 's learned expert-suboptimal distinctions. We provide LC-DP details in Section E and full algorithms for both methods in Section B.

5 Experiments

5.1 Environments

For evaluation, we use diverse continuous-control environments spanning navigation, driving, and manipulation, with varying horizon length, action precision, multimodality, and state-action dimensionality. Figure 3 shows the experimental tasks. For each task, we collect an expert dataset \mathcal{D}_E and a general dataset \mathcal{D}_G ; details are provided in Section F and G.

- **MAZE**: A navigation task [80] where an agent applies x/y forces to traverse a maze toward a sampled goal, observing its position, velocity, and the goal location.
- **PARKING**: A driving task [84] where an agent parks in a target spot via throttle and steering.
- **SWEEP** and **BOX-CLOSE**: MetaWorld [85] manipulation tasks where a Sawyer robot sweeps a block to a target and places a lid onto a box, respectively.
- **BLOCKPUSH**: A multistage task [47] requiring the robot to push two blocks into two target zones. Multiple valid strategies make this task inherently multimodal.
- **PEGINSERT**: A high-precision task [86] requiring joint-level control to insert a peg into a tightly matched side hole, demanding fine-grained corrective feedback.
- **HAMMER** and **RELOCATE**: High-dimensional Adroit dexterous hand tasks [87] involving hammering a nail and relocating a ball.

5.2 Task performance

We first evaluate whether additional language label supervision can better leverage general demonstrations in the suboptimal IL setting. Given a small expert dataset \mathcal{D}_E and a broader general dataset \mathcal{D}_G , the key challenge is to identify which suboptimal behaviors are useful for imitation. This experiment tests our central claim that language label provides more expressive behavioral feedback than scalar signals such as rewards, expert-likeness weights, or discriminator scores. We compare LC-BC and LC-DP against representative IL from suboptimal demonstrations:

- **BC** [1]: Behavior cloning that maximizes expert action likelihood using expert data only.
- **DWBC** [20]: A discriminator-weighted variant of BC that learns a discriminator to distinguish expert from non-expert data and reweights the imitation loss accordingly.
- **DemoDICE** [17]: An offline imitation method that matches stationary distributions with a KL regularizer toward general data, favoring expert-like state-action visitations.
- **ILID** [22]: An offline imitation learning method selecting demonstrations whose resulting states lie within the expert state manifold, and then performs BC on both the expert and selected data.
- **DP** [42]: A diffusion-policy baseline that models the action distribution with a conditional denoising process, trained on the expert dataset only.
- **LPB-Offline**: An offline adaptation of LPB [88], which leverages a dynamic model trained on general data to guide the DP near demonstrated behaviors.
- **LC-BC-reward** and **LC-DP-reward**: Reward-critique variants that reduce language label to scalar rewards under a LC-loss-style objective, collapsing all linguistic structure into a single numerical signal. See Section H.1 for details.
- **LC-BC-classifier** and **LC-DP-classifier**: Class-critique variants that reduce language label to discrete categorical labels mirroring the $\langle T \rangle$, $\langle A \rangle$, $\langle M \rangle$ structure, preserving multi-dimensionality but discarding natural-language expressiveness. See Section H.2 for details.

As shown in Table 1, our LC-BC and its variants outperform or match feedforward baselines across most environments, with the largest gains on multimodal tasks and those with larger test-time distribution shift, *e.g.*, out-of-distribution object or target positions. On BLOCKPUSH, LC-BC improves over BC from 34.4% to 47.2%, indicating that language label distinguishes multimodal demonstrations that scalar signals cannot separate. On manipulation tasks, LC-BC outperforms BC and matches or exceeds DWBC, DemoDICE, and ILID, suggesting that language-critique supervision performs better under distribution shift than the scalar signals used by prior methods.

The same pattern carries over to diffusion—our LC-DP and its variants match or improve over DP and LPB-Offline on all tasks, with notable gains on manipulation tasks. On simpler tasks such as PARKING and MAZE, most methods already achieve near-saturated performance, limiting the gains from language-critique supervision. DemoDICE performs strongly on several tasks but degrades on BLOCKPUSH, suggesting that expert-likeness weighting can be brittle in multimodal or multistage settings. On the precision-control task PEGINSERT, LC-BC shows only modest improvement over BC, whereas LC-DP maintains a clear advantage over DP. This suggests that language labels are more effective for high-level behavioral guidance and are better integrated by diffusion policies through iterative denoising than by feedforward policies for fine-grained control.

Language-critique methods consistently outperform LC-BC-reward and LC-DP-reward, confirming that language label carries a richer signal than scalar rewards. The classifier variants reveal a subtler trade-off: LC-BC-classifier and LC-DP-classifier encode the same information as language label via categorical labels over $\langle T \rangle$, $\langle A \rangle$, $\langle M \rangle$, but discard natural-language expressiveness. While language label captures finer-grained distinctions in behavior quality, it also introduces lexical noise irrelevant to the action signal. Diffusion policies, whose denoising process is robust to such noise, fully exploit the added expressiveness—hence LC-DP consistently outperforms LC-DP-classifier. Feedforward policies are more sensitive to this noise, so LC-BC-classifier occasionally outperforms LC-BC.

Overall, the results show that our proposed language-critique imitation learning provides an effective supervision signal for learning from suboptimal demonstrations across various domains. The qualitative results in Section J (Figure 11 & Figure 12) show policy rollouts on PEGINSERT and BOX-CLOSE, comparing BC and LC-BC and the corresponding language label and LC-loss.

5.3 Learning from mixed-quality demonstrations without expert partition

We further relax the assumption of access to a clean expert partition, *i.e.*, separate expert and general datasets \mathcal{D}_E and \mathcal{D}_G . Specifically, we consider the mixed-quality setting [26, 89], where only a single offline dataset \mathcal{D}_G containing both expert and suboptimal trajectories is available, analogous to the offline RL setting without reward signals. We evaluate this setting on the SWEEP and BOX-CLOSE.

We construct pseudo-expert datasets by selecting sequences with N consecutive positive language labels (where $\langle A \rangle$ labels each action as positive); larger N ensures stricter alignment with ground-truth expert behavior. Although these datasets contain mixed-quality demonstrations, they are treated as the

Table 1: **Comparisons to offline IL methods.** We report the mean and standard deviation of success rates across eight tasks, evaluated with 50 environment rollouts and 5 training seeds. We pair feedforward policies with BC, DWBC, DemoDICE, LC-BC-reward, and LC-BC and diffusion policies with DP, LPB-Offline, LC-DP-reward, LC-DP. Best results are in **bold**; second-best are underlined. LC-BC and LC-DP achieve competitive performance relative to all baselines across different environments. (% omitted.)

METHOD	MAZE	PARKING	SWEEP	BOX-CLOSE	BLOCKPUSH	PEGINSERT	HAMMER	RELOCATE
BC	79.6 ± 4.8	96.4 ± 3.0	76.0 ± 14.6	54.8 ± 8.4	34.4 ± 3.3	66.4 ± 5.4	96.0 ± 3.7	70.8 ± 8.3
DWBC	85.2 ± 5.8	<u>98.0</u> ± 0.0	66.0 ± 6.3	64.8 ± 7.8	26.0 ± 4.2	60.8 ± 1.8	88.0 ± 9.9	48.0 ± 6.6
DEMODICE	78.0 ± 3.2	96.8 ± 1.1	68.4 ± 10.1	82.0 ± 6.3	3.6 ± 2.6	67.2 ± 6.1	<u>96.8</u> ± 7.2	65.2 ± 8.1
ILID	<u>82.4</u> ± 3.6	93.6 ± 1.7	92.4 ± 7.3	69.6 ± 15.3	28.4 ± 4.1	59.6 ± 2.6	90.4 ± 9.1	80.8 ± 6.9
LC-BC-REWARD	79.6 ± 4.8	96.8 ± 2.7	88.4 ± 7.0	63.6 ± 12.1	38.8 ± 5.8	63.6 ± 3.3	90.0 ± 6.9	65.6 ± 11.2
LC-BC-CLASSIFIER	78.0 ± 3.2	100.0 ± 0.0	85.2 ± 3.3	82.0 ± 14.4	<u>40.4</u> ± 6.1	65.2 ± 3.6	75.6 ± 9.8	66.8 ± 12.6
LC-BC (OURS)	81.6 ± 6.1	96.8 ± 2.7	<u>90.0</u> ± 5.8	<u>80.4</u> ± 4.6	47.2 ± 4.1	67.2 ± 5.4	99.2 ± 1.8	<u>71.2</u> ± 5.9
DP	94.4 ± 2.2	96.0 ± 0.0	94.0 ± 5.7	64.8 ± 5.0	83.6 ± 4.8	<u>53.6</u> ± 1.7	<u>79.2</u> ± 3.0	67.2 ± 24.2
LPB-OFFLINE	93.6 ± 2.2	95.6 ± 0.9	93.6 ± 7.1	<u>67.2</u> ± 7.8	78.0 ± 4.9	51.6 ± 5.0	74.4 ± 3.6	59.6 ± 27.2
LC-DP-REWARD	<u>94.0</u> ± 2.0	<u>96.4</u> ± 0.9	94.0 ± 5.8	58.4 ± 5.7	<u>85.2</u> ± 1.1	53.2 ± 2.7	76.0 ± 1.4	66.8 ± 21.8
LC-DP-CLASSIFIER	92.4 ± 2.2	97.6 ± 0.9	<u>96.0</u> ± 5.8	66.8 ± 4.1	82.8 ± 2.3	52.8 ± 1.8	77.6 ± 0.9	<u>68.0</u> ± 24.8
LC-DP (OURS)	94.4 ± 1.7	97.6 ± 1.7	96.8 ± 3.6	69.2 ± 6.7	88.0 ± 1.4	56.8 ± 2.7	80.0 ± 3.2	77.6 ± 4.1

Table 2: **Learning from mixed-quality demonstrations.** We relax the clean expert dataset assumption and use language-based heuristic filtering to extract varying levels of expert-quality data from the general dataset. We evaluate two tasks across four quality levels $N=\{2,3,5,10\}$, with expert accuracy shown in parentheses. Higher N indicates stricter filtering; expert accuracy measures the fraction of selected samples from the ground-truth expert dataset as a proxy for data quality. We report success rates over 50 rollouts and 3 seeds (% omitted). LC-BC and LC-DP remain competitive with all baselines across both environments and policy architectures.

METHOD	SWEEP				BOX-CLOSE			
	2 (22.7%)	3 (33.6%)	5 (51.9%)	10 (84.3%)	2 (32.9%)	3 (48.9%)	5 (68.4%)	10 (86.8%)
BC	53.3 ± 8.1	65.3 ± 7.0	72.7 ± 3.1	<u>94.7</u> ± 3.1	50.0 ± 4.0	55.3 ± 11.0	<u>87.3</u> ± 4.6	84.7 ± 2.3
DWBC	60.7 ± 8.1	69.3 ± 5.0	74.0 ± 4.0	84.0 ± 3.5	34.7 ± 2.3	52.7 ± 7.0	71.3 ± 3.1	80.0 ± 2.0
DEMODICE	66.7 ± 5.0	76.7 ± 8.3	87.3 ± 3.1	80.7 ± 8.3	<u>65.3</u> ± 15.5	61.3 ± 5.0	<u>87.3</u> ± 5.0	84.0 ± 5.3
ILID	68.7 ± 10.1	86.7 ± 8.1	80.7 ± 8.3	95.3 ± 8.1	68.0 ± 7.2	<u>63.3</u> ± 6.4	50.7 ± 43.9	88.0 ± 2.0
LC-BC-REWARD	52.0 ± 7.2	60.7 ± 4.6	76.0 ± 10.6	91.3 ± 7.0	58.7 ± 5.0	56.7 ± 13.3	82.0 ± 8.0	85.3 ± 5.0
LC-BC-CLASSIFIER	87.7 ± 2.3	<u>85.3</u> ± 9.2	<u>85.3</u> ± 13.3	78.7 ± 5.0	64.7 ± 4.2	64.7 ± 5.8	80.0 ± 7.2	<u>87.3</u> ± 6.4
LC-BC (OURS)	<u>72.0</u> ± 8.7	81.3 ± 4.6	84.0 ± 8.7	88.0 ± 5.3	71.3 ± 8.3	78.0 ± 3.5	88.7 ± 7.0	94.0 ± 2.0
DP	66.0 ± 3.5	<u>70.7</u> ± 1.2	86.0 ± 0.0	100.0 ± 0.0	56.0 ± 4.0	<u>91.3</u> ± 1.2	92.0 ± 2.0	95.3 ± 2.3
LPB-OFFLINE	47.3 ± 2.3	58.0 ± 2.0	73.3 ± 8.1	97.3 ± 2.3	54.0 ± 5.3	82.0 ± 4.0	86.7 ± 6.1	91.3 ± 4.6
LC-DP-REWARD	<u>64.7</u> ± 4.2	72.0 ± 2.0	<u>87.3</u> ± 1.2	98.7 ± 1.2	58.0 ± 3.5	86.0 ± 2.0	91.3 ± 1.2	95.3 ± 1.2
LC-DP-CLASSIFIER	<u>64.7</u> ± 3.1	70.0 ± 2.0	88.0 ± 2.0	100.0 ± 0.0	<u>58.7</u> ± 3.1	88.7 ± 1.2	<u>92.7</u> ± 2.3	96.0 ± 2.0
LC-DP (OURS)	62.7 ± 1.2	72.0 ± 5.3	88.0 ± 4.0	<u>99.3</u> ± 1.2	70.0 ± 2.0	92.0 ± 2.0	94.0 ± 0.0	96.7 ± 1.2

expert distribution \mathcal{D}_E during imitation learning. As shown in Table 2, we evaluate $N \in \{2, 3, 5, 10\}$, where expert accuracy—the proportion of ground-truth expert samples—serves as a quality proxy ranging from 22.7% to 86.8%. For consistency, all methods are trained on identical filtered partitions, though only our approach utilizes language label supervision during policy learning.

Table 2 demonstrates that LC-BC excels with low-to-medium quality data, outperforming baselines when expert accuracy is lowest. This indicates that language label provides critical fine-grained supervision when demonstrations are suboptimal. While DWBC and DemoDICE perform worse with noisy expert partitions, ILID remains competitive in several settings, and our method proves the most robust by learning directly from the language labels. For diffusion-based policies, LC-DP achieves state-of-the-art or competitive results, particularly on BOX-CLOSE. Ultimately, these results confirm that the proposed language-critique loss enables effective learning from mixed-quality data without requiring a clean expert split.

5.4 Language label ablation studies

We conduct a series of ablation studies to identify the contribution of each proposed component and compare our language label generator μ_g against a general-purpose VLM-based labeling pipeline.

Compositional ablation of language labels. We study how each proposed component of language labels contributes to policy learning on the task BOX-CLOSE. As shown in Table 3 (left), using all three components achieves the best average performance for both LC-BC and LC-DP, confirming that

Table 3: **Language label ablation.** We ablate language label on BOX-CLOSE, reporting success rates averaged over 50 environment rollouts and 5 training seeds (% omitted). **(Left)** Ablation over the three language label components—<T>: Task Progress, <A>: Action Optimality, and <M>: Movement Guidance—showing that all three provide complementary supervision and achieve the best performance. **(Right)** Comparison of μ_g versus OpenAI o4-mini language labels across different LLM-Captioner backbones and post-processing strategies (concise, and μ_g -style). μ_g -shuffled randomly permutes language labels within $\mathcal{D}_G^{\text{lang}}$, preserving format but destroying semantic accuracy; μ_g -verbose preserves semantic accuracy but replaces the format with verbose descriptions.

<T>	<A>	<M>	LC-BC	LC-DP	Language label	LLM-Captioner Backbone	LC-BC	LC-DP
×	×	✓	67.6 ± 8.3	56.0 ± 5.7	o4-mini	SmoLLM2-135M-Instruct	55.2 ± 15.1	63.6 ± 6.1
×	✓	×	69.6 ± 10.5	65.2 ± 8.1	o4-mini	SmoLLM2-360M-Instruct	61.6 ± 14.6	71.2 ± 12.1
✓	×	×	51.6 ± 4.3	66.4 ± 7.1	o4-mini concise	SmoLLM2-135M-Instruct	63.4 ± 10.5	62.4 ± 7.1
✓	✓	×	65.6 ± 9.5	62.4 ± 15.5	o4-mini μ_g -style	SmoLLM2-135M-Instruct	56.4 ± 13.4	62.4 ± 12.8
✓	×	✓	79.6 ± 10.8	62.0 ± 9.6	μ_g -shuffled	SmoLLM2-135M-Instruct	55.6 ± 13.5	62.4 ± 11.3
×	✓	✓	74.4 ± 15.3	62.8 ± 8.8	μ_g -verbose	SmoLLM2-135M-Instruct	68.0 ± 12.4	62.0 ± 10.7
✓	✓	✓	80.4 ± 4.6	69.2 ± 6.7	μ_g	SmoLLM2-135M-Instruct	80.4 ± 4.6	69.2 ± 6.7

task progress <T>, action optimality <A>, and movement guidance <M> provide an effective signal. For LC-BC, <A> and <M> are individually more useful than <T> alone, as they are more closely related to action selection, while LC-DP is well supervised by stage-level signals (<T>) alone; nevertheless, the full label remains the best to distinguish behaviors among the general demonstrations.

VLM-generated language labels. We investigate whether general-purpose vision-language models (VLMs) can replace our structured language generator μ_g on BOX-CLOSE. Table 3 (right) shows that replacing μ_g with o4-mini prompting yields limited gains when paired with a small SmoLLM2-135M-Instruct captioner: LC-BC reaches only 55.2% and LC-DP only 63.6%, comparable to semantically shuffled μ_g labels (55.6%).

We attribute this gap to two distinct factors. First, open-ended VLM labels are verbose, diverse, and redundant, which makes their distribution harder for the captioner μ_ϕ to model. Second, treating μ_g as a feature-aligned reference reveals substantial semantic inaccuracy: o4-mini agrees with μ_g on only 51.8% of <T>, 46.1% of <A>, and just 18.8% of <M> descriptions. The sharp drop on fine-grained movement guidance <M> indicates that current VLMs struggle with the precise spatial reasoning over state-action effects that accurate movement labels demand.

We identify two strategies targeting each factor. First, increasing captioner capacity to SmoLLM2-360M-Instruct better models the diverse VLM distribution, raising LC-BC to 61.6% and LC-DP to 71.2%—the latter even surpassing μ_g . Second, post-processing the o4-mini labels into a concise form improves LC-BC to 63.4% but does not help LC-DP, whereas rewriting them into a μ_g -style structured format performs worse (56.4% for LC-BC, 62.4% for LC-DP), confirming that surface-level structure or style alone is insufficient.

To further disentangle linguistic form from semantic content, we construct two controlled variants: μ_g -shuffled preserves the concise structured form but destroys semantic alignment, while μ_g -verbose preserves semantic correctness but rewrites labels into diverse, human-like language. For LC-BC, μ_g -verbose substantially outperforms μ_g -shuffled (68.0% vs. 55.6%), showing that semantic accuracy matters more than surface conciseness for feedforward policies; for LC-DP, μ_g -verbose gives no gain over shuffled labels, indicating that diffusion-policy training is instead more sensitive to label-distribution complexity and benefits from concise, well-modeled supervision.

This asymmetry is consistent with the language-vs-classifier analysis in Section 5.2: feedforward policies are more sensitive to lexical noise and benefit most from semantically accurate labels, while diffusion policies, whose denoising process is inherently robust to such noise, can tolerate noisier or more verbose supervision and instead benefit more from increased captioner capacity. Thus high-quality VLM labels can be useful when paired with a stronger captioner for DP, but μ_g remains the most reliable supervision source due to its inherent semantic consistency and feature-aligned structure. Given that the primary failure mode is inaccurate fine-grained movement guidance, we leave to future work the use of stronger VLMs with better spatial and temporal reasoning capabilities, which may close the gap to μ_g and enable a fully VLM-driven labeling pipeline. Please refer to Section I.1 for a further detailed analysis.

Table 4: **Comparisons to offline RL methods.** We report the mean and standard deviation of success rates across eight tasks, evaluated with 50 environment rollouts and 5 seeds. We compare feedforward baselines (CQL, TD3+BC), a sequence-modeling baseline (Decision Transformer; DT), and diffusion baselines (EDP). Best results are in **bold**; second-best are underlined. LC-BC achieves the best feedforward performance on all eight tasks, while LC-DP is best on five tasks.

METHOD	MAZE	PARKING	SWEEP	BOX-CLOSE	BLOCKPUSH	PEGINSERT	HAMMER	RELOCATE
CQL	30.0 ± 1.4	25.2 ± 3.0	4.0 ± 3.2	10.0 ± 10.3	0.0 ± 0.0	1.6 ± 0.9	50.8 ± 5.2	2.4 ± 2.2
TD3+BC	<u>81.2</u> ± 3.0	<u>93.6</u> ± 0.9	38.8 ± 6.7	56.8 ± 10.4	<u>41.2</u> ± 5.8	58.4 ± 3.6	<u>97.6</u> ± 5.4	41.6 ± 7.0
LC-BC (OURS)	81.6 ± 6.1	96.8 ± 2.7	90.0 ± 5.8	80.4 ± 4.6	47.2 ± 4.1	67.2 ± 5.4	99.2 ± 1.8	71.2 ± 5.9
DT	41.6 ± 4.3	39.2 ± 2.3	59.2 ± 7.7	42.0 ± 5.5	2.4 ± 0.9	40.4 ± 3.3	61.6 ± 12.8	11.6 ± 2.6
EDP	91.2 ± 1.1	<u>96.8</u> ± 1.1	98.4 ± 2.6	71.6 ± 5.2	82.0 ± 6.8	<u>56.0</u> ± 2.4	83.6 ± 3.3	44.0 ± 5.1
LC-DP (OURS)	94.4 ± 1.7	97.6 ± 1.7	<u>96.8</u> ± 3.6	<u>69.2</u> ± 6.7	88.0 ± 1.4	56.8 ± 2.7	<u>80.0</u> ± 3.2	77.6 ± 4.1

5.5 Comparing to offline RL algorithms

We examine whether our language labels can capture behavioral information that standard value-learning methods fail to recover from scalar reward signals by comparing against offline RL algorithms spanning four families: value-based (CQL [27]), policy-regularized (TD3+BC [29]), sequence modeling (Decision Transformer, DT [28]), and diffusion-based (EDP [30]). LC-BC and LC-DP learn from language labels directly, while these baselines use scalar rewards converted from language labels following Cao et al. [38].

Table 4 shows LC-BC and LC-DP consistently match or outperform offline RL baselines. LC-BC outperforms TD3+BC on nearly all tasks, with particularly large gains on complex manipulation tasks, *e.g.*, BOX-CLOSE, BLOCKPUSH, RELOCATE. While TD3+BC performs competitively on simpler tasks, its reliance on value estimation limits its ability to leverage suboptimal data. In the diffusion setting, LC-DP achieves the best or near-best performance across most tasks, with notable improvements on long-horizon tasks such as BLOCKPUSH and high-dimensional task RELOCATE.

6 Conclusion

We introduced a language-critique framework for imitation learning from suboptimal demonstrations, which constructs critiques describing progress, failures, and corrective actions, and trains policies via a language-critique loss without reducing language to scalars, instantiated as LC-BC and LC-DP with theoretical guarantees on the expert-performance gap. Across diverse continuous-control tasks, our method consistently outperforms imitation and offline RL baselines. These results show that language provides an expressive and effective supervision signal for learning robust policies from suboptimal data. Broader impacts and limitations of our work are discussed in Section K and L, respectively.

Acknowledgments

This work was supported in part by the National Science and Technology Council, Taiwan, under Grants 114-2628-E-002-021-, 114-2628-E-A49-002, 115-2634-F-002-012-, and 115-2223-E-002-005-MY3, and the Taiwan Centers of Excellence in Artificial Intelligence. Shao-Hua Sun was supported by the Yushan Fellow Program of the Ministry of Education, Taiwan.

References

- [1] Dean A. Pomerleau. Alvin: An autonomous land vehicle in a neural network. In *Advances in Neural Information Processing Systems*, 1988.
- [2] Stefan Schaal. Learning from demonstration. In *Advances in Neural Information Processing Systems*, 1996.
- [3] Ahmed Hussein, Mohamed Medhat Gaber, Eyad Elyan, and Chrisina Jayne. Imitation learning: A survey of learning methods. *ACM Computing Surveys (CSUR)*, 50, 2017.
- [4] Ajay Mandlekar, Danfei Xu, Roberto Martín-Martín, Silvio Savarese, and Li Fei-Fei. Gti: Learning to generalize across long-horizon tasks from human demonstrations. In *Robotics: Science and Systems*, 2020.

- [5] Shang-Fu Chen, Hsiang-Chun Wang, Ming-Hao Hsu, Chun-Mao Lai, and Shao-Hua Sun. Diffusion model-augmented behavioral cloning. In *International Conference on Machine Learning*, 2024.
- [6] Stéphane Ross and J Andrew Bagnell. Efficient reductions for imitation learning. In *Proceedings of the thirteenth international conference on artificial intelligence and statistics*, 2010.
- [7] Stéphane Ross, Geoffrey Gordon, and J Andrew Bagnell. A reduction of imitation learning and structured prediction to no-regret online learning. In *Proceedings of the fourteenth international conference on artificial intelligence and statistics*, 2011.
- [8] Takayuki Osa, Joni Pajarinen, Gerhard Neumann, J Andrew Bagnell, Pieter Abbeel, and Jan Peters. An algorithmic perspective on imitation learning. *Foundations and Trends® in Robotics*, 7, 2018.
- [9] Jonathan Ho and Stefano Ermon. Generative adversarial imitation learning. In *Neural Information Processing Systems*, 2016.
- [10] Justin Fu, Katie Luo, and Sergey Levine. Learning robust rewards with adversarial inverse reinforcement learning. In *International Conference on Learning Representations*, 2018.
- [11] Youngwoon Lee, Andrew Szot, Shao-Hua Sun, and Joseph J. Lim. Generalizable imitation learning from observation via inferring goal proximity. In *Neural Information Processing Systems*, 2021.
- [12] Ilya Kostrikov, Ofir Nachum, and Jonathan Tompson. Imitation learning via off-policy distribution matching. In *International Conference on Learning Representations*, 2020.
- [13] Chun-Mao Lai, Hsiang-Chun Wang, Ping-Chun Hsieh, Yu-Chiang Frank Wang, Min-Hung Chen, and Shao-Hua Sun. Diffusion-reward adversarial imitation learning. In *Neural Information Processing Systems*, 2024.
- [14] Bo-Ruei Huang, Chun-Kai Yang, Chun-Mao Lai, Dai-Jie Wu, and Shao-Hua Sun. Diffusion imitation from observation. In *Neural Information Processing Systems*, 2024.
- [15] Fumihiko Sasaki and Ryota Yamashina. Behavioral cloning from noisy demonstrations. In *International Conference on Learning Representations*, 2021.
- [16] Lantao Yu, Tianhe Yu, Jiaming Song, Willie Neiswanger, and Stefano Ermon. Offline imitation learning with suboptimal demonstrations via relaxed distribution matching. In *Association for the Advancement of Artificial Intelligence*, 2023.
- [17] Geon-Hyeong Kim, Seokin Seo, Jongmin Lee, Wonseok Jeon, HyeongJoo Hwang, Hongseok Yang, and Kee-Eung Kim. DemoDICE: Offline imitation learning with supplementary imperfect demonstrations. In *International Conference on Learning Representations*, 2022.
- [18] Yunke Wang, Chang Xu, Bo Du, and Honglak Lee. Learning to weight imperfect demonstrations. In *International Conference on Machine Learning*, 2021.
- [19] Songyuan Zhang, Zhangjie Cao, Dorsa Sadigh, and Yanan Sui. Confidence-aware imitation learning from demonstrations with varying optimality. In *Neural Information Processing Systems*, 2021.
- [20] Haoran Xu, Xianyuan Zhan, Honglei Yin, and Huiling Qin. Discriminator-weighted offline imitation learning from suboptimal demonstrations. In *International Conference on Machine Learning*, 2022.
- [21] Yunke Wang, Minjing Dong, Yukun Zhao, Bo Du, and Chang Xu. Imitation learning from purified demonstrations. In *International Conference on Machine Learning*, 2024.
- [22] Sheng Yue, Jiani Liu, Xingyuan Hua, Ju Ren, Sen Lin, Junshan Zhang, and Yaoxue Zhang. How to leverage diverse demonstrations in offline imitation learning. In *International Conference on Machine Learning*, 2024.

- [23] Mengjiao Yang, Sergey Levine, and Ofir Nachum. TRAIL: Near-optimal imitation learning with suboptimal data. In *International Conference on Learning Representations*, 2022.
- [24] Yueh-Hua Wu, Nontawat Charoenphakdee, Han Bao, Voot Tangkaratt, and Masashi Sugiyama. Imitation learning from imperfect demonstration. In *International Conference on Machine Learning*, 2019.
- [25] Shang-Fu Chen, Co Yong, and Shao-Hua Sun. Restoring noisy demonstration for imitation learning with diffusion models. *IEEE Transactions on Neural Networks and Learning Systems*, 37:401–413, 2026.
- [26] Sergey Levine, Aviral Kumar, George Tucker, and Justin Fu. Offline reinforcement learning: Tutorial, review, and perspectives on open problems. *arXiv preprint arXiv:2005.01643*, 2020.
- [27] Aviral Kumar, Aurick Zhou, George Tucker, and Sergey Levine. Conservative q-learning for offline reinforcement learning. In *Neural Information Processing Systems*, 2020.
- [28] Lili Chen, Kevin Lu, Aravind Rajeswaran, Kimin Lee, Aditya Grover, Misha Laskin, Pieter Abbeel, Aravind Srinivas, and Igor Mordatch. Decision transformer: Reinforcement learning via sequence modeling. In *Neural Information Processing Systems*, 2021.
- [29] Scott Fujimoto and Shixiang Shane Gu. A minimalist approach to offline reinforcement learning. In *Neural Information Processing Systems*, 2021.
- [30] Bingyi Kang, Xiao Ma, Chao Du, Tianyu Pang, and Shuicheng Yan. Efficient diffusion policies for offline reinforcement learning. In *Neural Information Processing Systems*, 2023.
- [31] Sanja Fidler et al. Teaching machines to describe images with natural language feedback. In *Neural Information Processing Systems*, 2017.
- [32] Jesse Zhang, Karl Pertsch Jiahui Zhang, Ziyi Liu, Xiang Ren, Minsuk Chang, Shao-Hua Sun, and Joseph J. Lim. Bootstrap your own skills: Learning to solve new tasks with large language model guidance. In *Conference on Robot Learning*, 2023.
- [33] Ching-An Cheng, Andrey Kolobov, Dipendra Misra, Allen Nie, and Adith Swaminathan. LLF-bench: Benchmark for interactive learning from language feedback. In *ICLR 2024 Workshop on Large Language Model (LLM) Agents*, 2024.
- [34] Angelica Chen, Jérémy Scheurer, Jon Ander Campos, Tomasz Korbak, Jun Shern Chan, Samuel R Bowman, Kyunghyun Cho, and Ethan Perez. Learning from natural language feedback. *Transactions on machine learning research*, 2024.
- [35] Xidong Feng, Bo Liu, Ziyu Wan, Haotian Fu, Girish A. Koushik, Zhiyuan Hu, Mengyue Yang, Ying Wen, and Jun Wang. Natural language reinforcement learning. In *Scaling Self-Improving Foundation Models without Human Supervision*, 2025.
- [36] Yoonho Lee, Joseph Boen, and Chelsea Finn. Feedback descent: Open-ended text optimization via pairwise comparison. *arXiv preprint arXiv:2511.07919*, 2025.
- [37] Max Liu, Chan-Hung Yu, Wei-Hsu Lee, Cheng-Wei Hung, Yen-Chun Chen, and Shao-Hua Sun. Synthesizing programmatic reinforcement learning policies with large language model guided search. In *International Conference on Learning Representations*, 2025.
- [38] Meng Cao, Lei Shu, Lei Yu, Yun Zhu, Nevan Wichers, Yinxiao Liu, and Lei Meng. Enhancing reinforcement learning with dense rewards from language model critic. In *Empirical Methods in Natural Language Processing*, 2024.
- [39] Yufei Wang, Zhanyi Sun, Jesse Zhang, Zhou Xian, Erdem Biyik, David Held, and Zackory Erickson. RL-vlm-f: Reinforcement learning from vision language foundation model feedback. In *International Conference on Machine Learning*, 2024.
- [40] Pingcheng Jian, Xiao Wei, Yanbaihui Liu, Samuel A. Moore, Michael M. Zavlanos, and Boyuan Chen. LAPP: Large language model feedback for preference-driven reinforcement learning. *Transactions on Machine Learning Research*, 2025.

- [41] Belen Martin Urcelay, Andreas Krause, and Giorgia Ramponi. From words to rewards: Leveraging natural language for reinforcement learning. In *The Exploration in AI Today Workshop at ICML 2025*, 2025.
- [42] Cheng Chi, Zhenjia Xu, Siyuan Feng, Eric Cousineau, Yilun Du, Benjamin Burchfiel, Russ Tedrake, and Shuran Song. Diffusion policy: Visuomotor policy learning via action diffusion. In *Robotics: Science and Systems*, 2023.
- [43] Sham Kakade and John Langford. Approximately optimal approximate reinforcement learning. In *International Conference on Machine Learning*, 2002.
- [44] Chi Jin, Zhuoran Yang, Zhaoran Wang, and Michael I Jordan. Provably efficient reinforcement learning with linear function approximation. *Mathematics of Operations Research*, 48, 2023.
- [45] Nur Muhammad Shafiullah, Zichen Cui, Ariuntuya Arty Altanzaya, and Lerrel Pinto. Behavior transformers: Cloning k modes with one stone. In *Neural Information Processing Systems*, 2022.
- [46] Daniel S Brown, Wonjoon Goo, and Scott Niekum. Better-than-demonstrator imitation learning via automatically-ranked demonstrations. In *Conference on Robot Learning*, 2019.
- [47] Pete Florence, Corey Lynch, Andy Zeng, Oscar A Ramirez, Ayzaan Wahid, Laura Downs, Adrian Wong, Johnny Lee, Igor Mordatch, and Jonathan Tompson. Implicit behavioral cloning. In *Conference on Robot Learning*, 2021.
- [48] Joe Watson, Sandy Huang, and Nicolas Heess. Coherent soft imitation learning. In *Neural Information Processing Systems*, 2023.
- [49] Siliang Zeng, Chenliang Li, Alfredo Garcia, and Mingyi Hong. When demonstrations meet generative world models: A maximum likelihood framework for offline inverse reinforcement learning. In *Neural Information Processing Systems*, 2023.
- [50] Daniel Brown, Wonjoon Goo, Prabhat Nagarajan, and Scott Niekum. Extrapolating beyond suboptimal demonstrations via inverse reinforcement learning from observations. In *International Conference on Machine Learning*, 2019.
- [51] Letian Chen, Rohan Paleja, and Matthew Gombolay. Learning from suboptimal demonstration via self-supervised reward regression. In *Conference on Robot Learning*, 2020.
- [52] Tim Pearce, Tabish Rashid, Anssi Kanervisto, Dave Bignell, Mingfei Sun, Raluca Georgescu, Sergio Valcarcel Macua, Shan Zheng Tan, Ida Momennejad, Katja Hofmann, and Sam Devlin. Imitating human behaviour with diffusion models. In *International Conference on Learning Representations*, 2023.
- [53] Moritz Reuss, Maximilian Li, Xiaogang Jia, and Rudolf Lioutikov. Goal conditioned imitation learning using score-based diffusion policies. In *Robotics: Science and Systems*, 2023.
- [54] Moritz Reuss, Ömer Erdiñç Yağmurlu, Fabian Wenzel, and Rudolf Lioutikov. Multimodal diffusion transformer: Learning versatile behavior from multimodal goals. In *Robotics: Science and Systems*, 2024.
- [55] Sascha Lange, Thomas Gabel, and Martin Riedmiller. Batch reinforcement learning. In *Reinforcement learning: State-of-the-art*. Springer, 2012.
- [56] Ilya Kostrikov, Ashvin Nair, and Sergey Levine. Offline reinforcement learning with implicit q-learning. In *International Conference on Learning Representations*, 2022.
- [57] Gaon An, Seungyong Moon, Jang-Hyun Kim, and Hyun Oh Song. Uncertainty-based offline reinforcement learning with diversified q-ensemble. In *Neural Information Processing Systems*, 2021.
- [58] Xingyu Jiang, Ning Gao, Xiuhui Zhang, Hongkun Dou, and Yue Deng. Value-aligned behavior cloning for offline reinforcement learning via bi-level optimization. In *International Conference on Learning Representations*, 2025.

- [59] Yihao Sun, Jiayi Zhang, Chengxing Jia, Haoxin Lin, Junyin Ye, and Yang Yu. Model-bellman inconsistency for model-based offline reinforcement learning. In *International Conference on Machine Learning*, 2023.
- [60] Kwanyoung Park and Youngwoon Lee. Model-based offline reinforcement learning with lower expectile q-learning. In *International Conference on Learning Representations*, 2025.
- [61] Yunpeng Qing, Shunyu Liu, Jingyuan Cong, Kaixuan Chen, Yihe Zhou, and Mingli Song. A2po: Towards effective offline reinforcement learning from an advantage-aware perspective. In *Neural Information Processing Systems*, 2024.
- [62] Zhendong Wang, Jonathan J Hunt, and Mingyuan Zhou. Diffusion policies as an expressive policy class for offline reinforcement learning. In *International Conference on Learning Representations*, 2023.
- [63] Chen-Xiao Gao, Chenyang Wu, Mingjun Cao, Chenjun Xiao, Yang Yu, and Zongzhang Zhang. Behavior-regularized diffusion policy optimization for offline reinforcement learning. In *International Conference on Machine Learning*, 2025.
- [64] Philippe Hansen-Estruch, Ilya Kostrikov, Michael Janner, Jakub Grudzien Kuba, and Sergey Levine. Idql: Implicit q-learning as an actor-critic method with diffusion policies. *arXiv preprint arXiv:2304.10573*, 2023.
- [65] Cheng Lu, Huayu Chen, Jianfei Chen, Hang Su, Chongxuan Li, and Jun Zhu. Contrastive energy prediction for exact energy-guided diffusion sampling in offline reinforcement learning. In *International Conference on Machine Learning*, 2023.
- [66] Chang Chen, Fei Deng, Kenji Kawaguchi, Caglar Gulcehre, and Sungjin Ahn. Simple hierarchical planning with diffusion. In *International Conference on Learning Representations*, 2024.
- [67] Donghyeon Ki, JunHyeok Oh, Seong-Woong Shim, and Byung-Jun Lee. Prior-guided diffusion planning for offline reinforcement learning. In *Neural Information Processing Systems*, 2025.
- [68] Lucy Xiaoyang Shi, Zheyuan Hu, Tony Z Zhao, Archit Sharma, Karl Pertsch, Jianlan Luo, Sergey Levine, and Chelsea Finn. Yell at your robot: Improving on-the-fly from language corrections. In *Robotics: Science and Systems*, 2024.
- [69] Corey Lynch and Pierre Sermanet. Language conditioned imitation learning over unstructured data. In *Robotics: Science and Systems*, 2021.
- [70] Simon Stepputtis, Joseph Campbell, Mariano Phielipp, Stefan Lee, Chitta Baral, and Heni Ben Amor. Language-conditioned imitation learning for robot manipulation tasks. In *Neural Information Processing Systems*, 2020.
- [71] Shao-Hua Sun, Hyeonwoo Noh, Sriram Somasundaram, and Joseph J. Lim. Neural program synthesis from diverse demonstration videos. In *International Conference on Machine Learning*, 2018.
- [72] Shao-Hua Sun, Te-Lin Wu, and Joseph J. Lim. Program guided agent. In *International Conference on Learning Representations*, 2020.
- [73] Guan-Ting Liu, En-Pei Hu, Pu-Jen Cheng, Hung-Yi Lee, and Shao-Hua Sun. Hierarchical programmatic reinforcement learning via learning to compose programs. In *International Conference on Machine Learning*, 2023.
- [74] Yu-An Lin, Chen-Tao Lee, Chih-Han Yang, Guan-Ting Liu, and Shao-Hua Sun. Hierarchical programmatic option framework. In *Neural Information Processing Systems*, 2023.
- [75] Karl Moritz Hermann, Felix Hill, Simon Green, Fumin Wang, Ryan Faulkner, Hubert Soyer, David Szepesvari, Wojciech Marian Czarnecki, Max Jaderberg, Denis Teplyashin, et al. Grounded language learning in a simulated 3d world. *arXiv preprint arXiv:1706.06551*, 2017.

- [76] Yinpei Dai, Jayjun Lee, Nima Fazeli, and Joyce Chai. Racer: Rich language-guided failure recovery policies for imitation learning. In *International Conference on Robotics and Automation*, 2025.
- [77] Wanqiao Xu, Allen Nie, Ruijie Zheng, Aditya Modi, Adith Swaminathan, and Ching-An Cheng. Provably learning from language feedback. In *The Exploration in AI Today Workshop at ICML 2025*, 2025.
- [78] Jiajun Xi, Yinong He, Jianing Yang, Yinpei Dai, and Joyce Chai. Teaching embodied reinforcement learning agents: Informativeness and diversity of language use. In *Empirical Methods in Natural Language Processing*, 2024.
- [79] Wenhao Yu, Nimrod Gileadi, Chuyuan Fu, Sean Kirmani, Kuang-Huei Lee, Montserrat Gonzalez Arenas, Hao-Tien Lewis Chiang, Tom Erez, Leonard Hasenclever, Jan Humplik, et al. Language to rewards for robotic skill synthesis. In *Conference on Robot Learning*, 2023.
- [80] Justin Fu, Aviral Kumar, Ofir Nachum, George Tucker, and Sergey Levine. D4rl: Datasets for deep data-driven reinforcement learning. *arXiv preprint arXiv:2004.07219*, 2020.
- [81] Jiahui Zhang, Yusen Luo, Abrar Anwar, Sumedh Anand Sontakke, Joseph J Lim, Jesse Thomason, Erdem Biyik, and Jesse Zhang. Rewind: Language-guided rewards teach robot policies without new demonstrations. In *Conference on Robot Learning*, 2025.
- [82] Andrew Y Ng, Daishi Harada, and Stuart Russell. Policy invariance under reward transformations: Theory and application to reward shaping. In *International Conference on Machine Learning*, 1999.
- [83] Olaf Ronneberger, Philipp Fischer, and Thomas Brox. U-net: Convolutional networks for biomedical image segmentation. In *International Conference on Medical image computing and computer-assisted intervention*, 2015.
- [84] Edouard Leurent. An environment for autonomous driving decision-making, 2018.
- [85] Tianhe Yu, Deirdre Quillen, Zhanpeng He, Ryan Julian, Karol Hausman, Chelsea Finn, and Sergey Levine. Meta-world: A benchmark and evaluation for multi-task and meta reinforcement learning. In *Conference on Robot Learning*, 2019.
- [86] Stone Tao, Fanbo Xiang, Arth Shukla, Yuzhe Qin, Xander Hinrichsen, Xiaodi Yuan, Chen Bao, Xinsong Lin, Yulin Liu, Tse-Kai Chan, Yuan Gao, Xuanlin Li, Tongzhou Mu, Nan Xiao, Arnav Gurha, Viswesh N, Yong Woo Choi, Yen-Ru Chen, Zhiao Huang, Roberto Calandra, Rui Chen, Shan Luo, and Hao Su. Maniskill3: GPU parallelized robot simulation and rendering for generalizable embodied AI. In *7th Robot Learning Workshop: Towards Robots with Human-Level Abilities*, 2025.
- [87] Aravind Rajeswaran, Vikash Kumar, Abhishek Gupta, Giulia Vezzani, John Schulman, Emanuel Todorov, and Sergey Levine. Learning complex dexterous manipulation with deep reinforcement learning and demonstrations. In *Robotics: Science and Systems*, 2018.
- [88] Zhanyi Sun and Shuran Song. Latent policy barrier: Learning robust visuomotor policies by staying in-distribution. In *Neural Information Processing Systems*, 2025.
- [89] Minghuan Liu, Hanye Zhao, Zhengyu Yang, Jian Shen, Weinan Zhang, Li Zhao, and Tie-Yan Liu. Curriculum offline imitating learning. In *Neural Information Processing Systems*, 2021.
- [90] André Barreto, Will Dabney, Rémi Munos, Jonathan J Hunt, Tom Schaul, Hado P Van Hasselt, and David Silver. Successor features for transfer in reinforcement learning. In *Neural Information Processing Systems*, 2017.
- [91] Pieter Abbeel and Andrew Y Ng. Apprenticeship learning via inverse reinforcement learning. In *International Conference on Machine Learning*, 2004.
- [92] Loubna Ben Allal, Anton Lozhkov, Elie Bakouch, Gabriel Martín Blázquez, Guilherme Penedo, Lewis Tunstall, Andrés Marafioti, Hynek Kydlíček, Agustín Piqueres Lajarín, Vaibhav Srivastav, et al. Smollm2: When smol goes big—data-centric training of a small language model. *arXiv preprint arXiv:2502.02737*, 2025.

- [93] Theodore Sumers, Kenneth Marino, Arun Ahuja, Rob Fergus, and Ishita Dasgupta. Distilling internet-scale vision-language models into embodied agents. In *International Conference on Machine Learning*, 2023.
- [94] Danny Driess, Fei Xia, Mehdi SM Sajjadi, Corey Lynch, Aakanksha Chowdhery, Ayzaan Wahid, Jonathan Tompson, Quan Vuong, Tianhe Yu, Wenlong Huang, et al. Palm-e: An embodied multimodal language model. In *International Conference on Machine Learning*, 2023.
- [95] Joshua Jones, Oier Mees, Carmelo Sferrazza, Kyle Stachowicz, Pieter Abbeel, and Sergey Levine. Beyond sight: Finetuning generalist robot policies with heterogeneous sensors via language grounding. In *International Conference on Robotics and Automation*, 2025.
- [96] Jonathan Ho, Ajay Jain, and Pieter Abbeel. Denoising diffusion probabilistic models. In *Neural Information Processing Systems*, 2020.
- [97] Tuomas Haarnoja, Aurick Zhou, Pieter Abbeel, and Sergey Levine. Soft actor-critic: Off-policy maximum entropy deep reinforcement learning with a stochastic actor. In *International Conference on Machine Learning*, 2018.
- [98] John Schulman, Filip Wolski, Prafulla Dhariwal, Alec Radford, and Oleg Klimov. Proximal policy optimization algorithms. *arXiv preprint arXiv:1707.06347*, 2017.
- [99] Rodrigo de Lazcano, Kallinteris Andreas, Jun Jet Tai, Seungjae Ryan Lee, and Jordan Terry. Gymnasium robotics, 2024. URL <http://github.com/Farama-Foundation/Gymnasium-Robotics>.
- [100] An Yang, Baosong Yang, Binyuan Hui, Bo Zheng, Bowen Yu, Chang Zhou, Chengpeng Li, Chengyuan Li, Dayiheng Liu, Fei Huang, et al. Qwen2 technical report. *eprint arXiv:2407.10671*, 2024.
- [101] Albert Q Jiang, Alexandre Sablayrolles, Arthur Mensch, Chris Bamford, Devendra Singh Chaplot, Diego de las Casas, Florian Bressand, Gianna Lengyel, Guillaume Lample, Lucile Saulnier, et al. Mistral 7b. *arXiv preprint arXiv:2310.06825*, 2023.

Appendix

Table of Contents

A Theoretical Analysis	17
A.1 Expert-state language-critique objective	18
A.2 Language-critique gap as distribution matching	18
A.3 Language-critique gap bounds feature gap	19
A.4 Proof of the performance difference bound	19
A.5 Connection to the practical LC-loss	20
B Algorithm	22
C Language label details	23
D LLM-Captioner details	27
E LC-DP details	28
E.1 Diffusion model: forward and reverse process	28
E.2 Diffusion model: training algorithm	29
E.3 Reweighting factor derivation	30
F Environment and tasks details	33
G Training details	34
G.1 Model architectures	34
G.2 Hyperparameters	37
G.3 Computational resources	38
H Baseline details	39
H.1 LC-BC-reward and LC-DP-reward	39
H.2 LC-BC-classifier and LC-DP-classifier	40
I Additional experimental results	42
I.1 VLM-generated language labels.	42
I.2 LLM-Captioner ablation	42
I.3 LLM-Captioner training data analysis	43
I.4 λ sensitivity	44
J Qualitative results of LC-loss and LLM-Captioner	44
K Impact statement	46
L Limitations	46

A Theoretical Analysis

In this section, we provide theoretical justification for the language-critique objective introduced in Section 4.1. We show that the expert-state language-critique gap naturally reflects the sub-optimality gap. Specifically, under mild assumptions, minimizing the language-critique gap $\Delta_{LC}(\pi_\theta)$ decreases an upper bound on the gap $J_{r^*}(\pi_E) - J_{r^*}(\pi_\theta)$. This provides a theoretical basis for using language label as an auxiliary imitation signal beyond action matching.

A.1 Expert-state language-critique objective

Our method uses both expert and suboptimal demonstrations, where suboptimal data may contain useful near-optimal behaviors as well as noisy rollouts that should be discounted. To identify useful behaviors, we need a unified measure of policy quality for both π_θ and the behavior policies underlying the demonstrations.

Formally, let $d_E^t(s) := \Pr(s_t = s \mid \pi_E)$ be the expert state distribution at timestep t , and let $A_{r,t}^\pi(s, a) := Q_{r,t}^\pi(s, a) - V_{r,t}^\pi(s)$ be the time-dependent advantage, where $Q_{r,t}^\pi$ and $V_{r,t}^\pi$ are the action- and state-value functions of π under reward r over the remaining horizon.

We build on the following performance difference lemma:

Lemma A.1 (Performance difference lemma.). *Following Kakade and Langford [43], the return difference between the expert policy and an arbitrary policy π , evaluated under the optimal reward r^* , admits the following decomposition:*

$$J_{r^*}(\pi_E) - J_{r^*}(\pi) = \sum_{t=0}^{T-1} \gamma^t \mathbb{E}_{s_t \sim d_E^t, a_t^E \sim \pi_E(\cdot | s_t)} [A_{r^*,t}^\pi(s_t, a_t^E)]. \quad (16)$$

This provides such a measure and motivates the objective introduced in Section 4.1, which we derive step by step in the remainder of this section.

For an expert state $s_t \sim d_E^t$, let $a_t^E \sim \pi_E(\cdot | s_t)$ denote the expert action. Given a language label function μ , the corresponding expert language label is sampled as

$$l_t^E \sim \mu(\cdot | s_t, a_t^E).$$

For a learned policy π_θ , we evaluate the policy action $\hat{a}_t \sim \pi_\theta(\cdot | s_t)$ by the likelihood with which it explains the same expert language label. We define the expert-state language-critique objective as

$$J_{\text{LC}}(\pi_\theta) := \sum_{t=0}^{T-1} \gamma^t \mathbb{E}_{s_t \sim d_E^t, a_t^E \sim \pi_E(\cdot | s_t), l_t^E \sim \mu(\cdot | s_t, a_t^E), \hat{a}_t \sim \pi_\theta(\cdot | s_t)} [\log \mu(l_t^E | s_t, \hat{a}_t)]. \quad (17)$$

where T is the horizon of each episode. Similarly, the expert policy obtains

$$J_{\text{LC}}(\pi_E) := \sum_{t=0}^{T-1} \gamma^t \mathbb{E}_{s_t \sim d_E^t, a_t^E \sim \pi_E(\cdot | s_t), l_t^E \sim \mu(\cdot | s_t, a_t^E)} [\log \mu(l_t^E | s_t, a_t^E)]. \quad (18)$$

The language-critique gap is defined as

$$\Delta_{\text{LC}}(\pi_\theta) := J_{\text{LC}}(\pi_E) - J_{\text{LC}}(\pi_\theta) \quad (19)$$

Since $J_{\text{LC}}(\pi_E)$ is independent of the learned policy, minimizing $\Delta_{\text{LC}}(\pi_\theta)$ is equivalent to maximizing $J_{\text{LC}}(\pi_\theta)$. Expanding $\Delta_{\text{LC}}(\pi_\theta)$, we obtain

$$\Delta_{\text{LC}}(\pi_\theta) = \sum_{t=0}^{T-1} \gamma^t \mathbb{E}_{s_t \sim d_E^t, a_t^E \sim \pi_E, l_t^E \sim \mu(\cdot | s_t, a_t^E), \hat{a}_t \sim \pi_\theta} [\log \mu(l_t^E | s_t, a_t^E) - \log \mu(l_t^E | s_t, \hat{a}_t)]. \quad (20)$$

A.2 Language-critique gap as distribution matching

First, we show that the language-critique gap $\Delta_{\text{LC}}(\pi_\theta)$ is exactly a KL divergence between the expert language label distribution and the policy-yielded language label distribution. Following the definition of KL divergence, we have:

$$D_{\text{KL}}(\mu(\cdot | s_t, a_t^E) \parallel \mu(\cdot | s_t, \hat{a}_t)) = \mathbb{E}_{l_t^E \sim \mu(\cdot | s_t, a_t^E)} \left[\log \frac{\mu(l_t^E | s_t, a_t^E)}{\mu(l_t^E | s_t, \hat{a}_t)} \right].$$

Therefore,

$$\Delta_{\text{LC}}(\pi_\theta) = \sum_{t=0}^{T-1} \gamma^t \mathbb{E}_{s_t \sim d_E^t, a_t^E \sim \pi_E(\cdot | s_t), \hat{a}_t \sim \pi_\theta(\cdot | s_t)} [D_{\text{KL}}(\mu(\cdot | s_t, a_t^E) \parallel \mu(\cdot | s_t, \hat{a}_t))]. \quad (21)$$

Therefore, minimizing $\Delta_{\text{LC}}(\pi_\theta)$ encourages the policy-induced language distribution $\mu(\cdot | s_t, \hat{a}_t)$ to match the expert-induced language distribution $\mu(\cdot | s_t, a_t^E)$ on expert states $s_t \sim d_E^t$.

A.3 Language-critique gap bounds feature gap

We now connect language distribution matching to feature matching. We assume the following:

Assumption A.2 (Linear realizability). For any policy π , the action-value function under the optimal task reward r^* is linear in a reward-relevant feature representation: there exist weights $w_t^\pi \in \mathbb{R}^d$ for each t such that $Q_{r^*,t}^{\pi}(s, a) = w_t^{\pi \top} \psi(s, a)$, where $\psi : \mathcal{S} \times \mathcal{A} \rightarrow \mathbb{R}^d$. We assume $w_{\max} := \sup_{\pi, t} \|w_t^\pi\|_2$ is finite.

Notably, this assumption is standard in the literature of linear MDPs [44] and successor features [90], and underlies feature-expectation matching in apprenticeship learning [91].

Assumption A.3 (Language-critique sufficiency). The language label preserves reward-relevant distinctions between actions: there exists $c > 0$ such that, for any state s and actions a, a' ,

$$D_{\text{KL}}(\mu(\cdot | s, a') \parallel \mu(\cdot | s, a)) \geq c \|\psi(s, a') - \psi(s, a)\|_2^2. \quad (22)$$

This assumption states that reward-relevant differences in the state-action feature space are reflected by the induced language distributions. The condition rules out uninformative labels and requires μ to preserve distinctions in the features of state-action $\psi(s, a) : \mathcal{S} \times \mathcal{A} \rightarrow \mathbb{R}^d$: if two actions a, a' in the same state differ, $\mu(\cdot | s, a)$ and $\mu(\cdot | s, a')$ shall be distinguishable. In our setting, this assumption is realized by the structured design of language label: the generated labels explicitly encode task progress, action optimality, and movement guidance, rather than arbitrary free-form descriptions. See Section 4.2.

Under Assumption A.3, the expected feature gap is bounded by the language-critique gap:

$$\sum_{t=0}^{T-1} \gamma^t \mathbb{E}_{s_t \sim d_E^t, a_t^E \sim \pi_E(\cdot | s_t), \hat{a}_t \sim \pi_\theta(\cdot | s_t)} \left[\|\psi(s_t, a_t^E) - \psi(s_t, \hat{a}_t)\|_2^2 \right] \leq \frac{1}{c} \Delta_{\text{LC}}(\pi_\theta). \quad (23)$$

A.4 Proof of the performance difference bound

Below we formally state the performance difference bound in Theorem A.4 with the detailed proof.

Theorem A.4 (Language-critique gap bounds the performance difference gap). *Under Assumptions A.2 and A.3, the performance difference between the expert policy π_E and the learned policy π_θ can be upper bounded by the expert-referenced language-critique gap:*

$$|J_{r^*}(\pi_E) - J_{r^*}(\pi_\theta)| \leq w_{\max} \sqrt{\frac{1}{c} \frac{1 - \gamma^T}{1 - \gamma} \Delta_{\text{LC}}(\pi_\theta)}. \quad (24)$$

Proof. By the performance difference lemma [43], we have

$$J_{r^*}(\pi_E) - J_{r^*}(\pi_\theta) = \sum_{t=0}^{T-1} \gamma^t \mathbb{E}_{s_t \sim d_E^t, a_t^E \sim \pi_E} [A_{r^*,t}^{\pi_\theta}(s_t, a_t^E)]. \quad (25)$$

Since $A_{r^*,t}^{\pi_\theta}(s, a) = Q_{r^*,t}^{\pi_\theta}(s, a) - V_{r^*,t}^{\pi_\theta}(s)$ and $V_{r^*,t}^{\pi_\theta}(s) = \mathbb{E}_{\hat{a} \sim \pi_\theta(\cdot | s)} [Q_{r^*,t}^{\pi_\theta}(s, \hat{a})]$, we have

$$\mathbb{E}_{a^E \sim \pi_E} [A_{r^*,t}^{\pi_\theta}(s, a^E)] = \mathbb{E}_{a^E \sim \pi_E, \hat{a} \sim \pi_\theta} [Q_{r^*,t}^{\pi_\theta}(s, a^E) - Q_{r^*,t}^{\pi_\theta}(s, \hat{a})]. \quad (26)$$

Under Assumption A.2, $Q_{r^*,t}^{\pi_\theta}(s, a) = w_t^{\pi_\theta \top} \psi(s, a)$, so

$$Q_{r^*,t}^{\pi_\theta}(s, a^E) - Q_{r^*,t}^{\pi_\theta}(s, \hat{a}) = w_t^{\pi_\theta \top} (\psi(s, a^E) - \psi(s, \hat{a})) = w_t^{\pi_\theta \top} X_t, \quad (27)$$

where $X_t := \psi(s_t, a_t^E) - \psi(s_t, \hat{a}_t)$. Plugging this back into Equation (25), we have

$$J_{r^*}(\pi_E) - J_{r^*}(\pi_\theta) = \sum_{t=0}^{T-1} \gamma^t \mathbb{E} [w_t^{\pi_\theta \top} X_t]. \quad (28)$$

By Jensen’s inequality, $\|\mathbb{E}[X_t]\|_2^2 \leq \mathbb{E}[\|X_t\|_2^2]$. Applying weighted Cauchy–Schwarz to the discounted sum,

$$\left\| \sum_{t=0}^{T-1} \gamma^t \mathbb{E}[X_t] \right\|_2^2 \leq \left(\sum_{t=0}^{T-1} \gamma^t \right) \left(\sum_{t=0}^{T-1} \gamma^t \mathbb{E}[\|X_t\|_2^2] \right) \leq \frac{1-\gamma^T}{1-\gamma} \sum_{t=0}^{T-1} \gamma^t \mathbb{E}[\|X_t\|_2^2]. \quad (29)$$

By Equation (23) (following Assumption A.3),

$$\sum_{t=0}^{T-1} \gamma^t \mathbb{E}[\|X_t\|_2^2] \leq \frac{1}{c} \Delta_{LC}(\pi_\theta). \quad (30)$$

Combining Equation (29) and Equation (30),

$$\sum_{t=0}^{T-1} \gamma^t \|\mathbb{E}[X_t]\|_2 \leq \sqrt{\frac{1}{c} \frac{1-\gamma^T}{1-\gamma} \Delta_{LC}(\pi_\theta)}. \quad (31)$$

Putting everything together,

$$|J_{r^*}(\pi_E) - J_{r^*}(\pi_\theta)| = \left| \sum_{t=0}^{T-1} \gamma^t \mathbb{E} \left[w_t^{\pi_\theta \top} X_t \right] \right| \quad (32)$$

$$\leq w_{\max} \left\| \sum_{t=0}^{T-1} \gamma^t \mathbb{E}[X_t] \right\|_2 \quad (33)$$

$$\leq w_{\max} \sum_{t=0}^{T-1} \gamma^t \|\mathbb{E}[X_t]\|_2 \quad (34)$$

$$\leq w_{\max} \sqrt{\frac{1}{c} \frac{1-\gamma^T}{1-\gamma} \Delta_{LC}(\pi_\theta)}, \quad (35)$$

which proves Theorem A.4. □

A.5 Connection to the practical LC-loss

The theoretical objective above is defined using the language-critique function μ . In practice, μ is instantiated in two stages. First, the language label generator μ_g produces structured language labels for the expert and general offline datasets. Second, the differentiable LLM-Captioner μ_ϕ is trained on $\mathcal{D}_G^{\text{lang}}$ to approximate these labels and is then frozen during policy training. In this subsection, we identify the relationship between the theoretical objective and the practical objective. First, we go through the details of the practical LC-loss.

For a language label $l_t = \{l_{t,1}, \dots, l_{t,N_t}\}$ of token length N_t , the token-level cross entropy loss under μ_ϕ is

$$\ell_{\text{CE}}^\phi(l_t, s_t, a_t) = -\frac{1}{N_t} \sum_{n=1}^{N_t} \log \mu_\phi(l_{t,n} | l_{t,<n}, s_t, a_t).$$

By the chain rule of conditional probability, this satisfies the exact identity:

$$\ell_{\text{CE}}^\phi(l_t, s_t, a_t) = -\frac{1}{N_t} \log \mu_\phi(l_t | s_t, a_t), \quad (36)$$

i.e., the token-averaged loss is exactly the sequence log-likelihood scaled by $1/N_t$. The dataset-level losses are:

$$\mathcal{L}_{\text{CE}}(\pi_\theta) = \mathbb{E}_{(s_t, l_t) \sim \mathcal{D}_E^{\text{lang}}, \hat{a}_t \sim \pi_\theta} \left[\ell_{\text{CE}}^\phi(l_t, s_t, \hat{a}_t) \right] \quad (37)$$

$$\mathcal{L}_{\text{CE}}(\pi_E) = \mathbb{E}_{(s_t, a_t^E, l_t) \sim \mathcal{D}_E^{\text{lang}}} \left[\ell_{\text{CE}}^\phi(l_t, s_t, a_t^E) \right] \quad (38)$$

$$\mathcal{L}_{\text{LC}}(\pi_\theta, \pi_E) = [\mathcal{L}_{\text{CE}}(\pi_\theta) - \text{sg}(\mathcal{L}_{\text{CE}}(\pi_E))]_+ \quad (39)$$

where $[x]_+ = \max(x, 0)$, and $\text{sg}(\cdot)$ denotes stop-gradient, and $\mathcal{L}_{\text{LC}}(\pi_\theta, \pi_E)$ is the token-level practical LC-loss. To formally connect \mathcal{L}_{LC} to Δ_{LC} , we introduce the following assumptions corresponding to three key aspects in terms of approximation: bounded language label lengths, μ_ϕ fidelity, and time-step t weighting.

Assumption A.5 (Bounded language label lengths). All the language labels yielded by μ_g have a limited length under some tokenization strategy. There exist constants $0 < N_{\min} \leq N_{\max} < \infty$ such that $N_{\min} \leq N_t \leq N_{\max}$ for all l_t in the $\mathcal{D}_E^{\text{lang}}$ and every policy sample.

Assumption A.6 (LLM-Captioner μ_ϕ approximation). Since the μ_ϕ approximation is not perfect, there exists $\epsilon_\phi \geq 0$ such that, for every $s_t \sim d_E^t$, $a_t \sim \pi(\cdot | s_t)$, and $l_t \sim \mu_g(\cdot | s_t, a_t)$,

$$|\log \mu_g(l_t | s_t, a_t) - \log \mu_\phi(l_t | s_t, a_t)| \leq \epsilon_\phi. \quad (40)$$

The constant ϵ_ϕ captures the distillation error introduced by replacing the generator μ_g with the differentiable LLM-Captioner μ_ϕ . It is small once μ_ϕ is trained to high fidelity on $\mathcal{D}_G^{\text{lang}}$.

Assumption A.7 (Time-step t coverage). Let p_t denote the empirical frequency of timestep t in $\mathcal{D}_E^{\text{lang}}$, and define $q_t := \gamma^t / p_t$. There exist constants $0 < q_{\min} \leq q_{\max} < \infty$ such that $q_{\min} \leq q_t \leq q_{\max}$ for all $t \in \{0, \dots, T-1\}$. In the undiscounted finite-horizon setting, where $\gamma = 1$ with uniform timestep coverage $p_t = 1/T$, $q_t = T$ exactly.

The above three assumptions are fairly mild and can be satisfied by our implementation in practice. We now combine these assumptions to bound the theoretical gap $\Delta_{\text{LC}}(\pi_\theta)$ by the practical loss $\mathcal{L}_{\text{LC}}(\pi_\theta, \pi_E)$. First, we define the captioner-based language critique gap, identical in form to $\Delta_{\text{LC}}(\pi_\theta)$, but using μ_ϕ instead of a general μ .

$$\Delta_{r,\phi}(\pi_\theta) := \sum_{t=0}^{T-1} \gamma^t \mathbb{E}_{s_t \sim d_E^t, a_t^E \sim \pi_E(\cdot | s_t), l_t^E \sim \mu_g, \hat{a}_t \sim \pi_\theta(\cdot | s_t)} [\log \mu_\phi(l_t^E | s_t, a_t^E) - \log \mu_\phi(l_t^E | s_t, \hat{a}_t)]. \quad (41)$$

We now bound $\Delta_{\text{LC}}(\pi_\theta)$ — instantiated with the generator $\mu = \mu_g$ — by $\Delta_{r,\phi}(\pi_\theta)$ using Assumption A.6. For every $(s_t, a_t, l_t) \in \mathcal{D}_E^{\text{lang}}$ and every policy sample \hat{a}_t , the assumption gives

$$|\log \mu_g(l_t^E | s_t, a_t^E) - \log \mu_\phi(l_t^E | s_t, a_t^E)| \leq \epsilon_\phi, \quad (42)$$

$$|\log \mu_g(l_t^E | s_t, \hat{a}_t) - \log \mu_\phi(l_t^E | s_t, \hat{a}_t)| \leq \epsilon_\phi. \quad (43)$$

Combining the two bounds we have,

$$[\log \mu_g(l_t^E | s_t, a_t^E) - \log \mu_g(l_t^E | s_t, \hat{a}_t)] \leq [\log \mu_\phi(l_t^E | s_t, a_t^E) - \log \mu_\phi(l_t^E | s_t, \hat{a}_t)] + 2\epsilon_\phi.$$

Taking the expectation under $s_t \sim d_E^t$, $a_t^E \sim \pi_E$, $l_t^E \sim \mu_g$, $\hat{a}_t \sim \pi_\theta$, and the discounted sum $\sum_t \gamma^t$ on both sides, we obtain

$$\Delta_{\text{LC}}(\pi_\theta) \leq \Delta_{r,\phi}(\pi_\theta) + 2\epsilon_\phi \sum_{t=0}^{T-1} \gamma^t = \Delta_{r,\phi}(\pi_\theta) + 2\epsilon_\phi \frac{1 - \gamma^T}{1 - \gamma}. \quad (44)$$

According to Equation (36) and Assumption A.5, we define a length-weighted gap for the LLM-style log-likelihood we have in practice:

$$\bar{\Delta}_{r,\phi}(\pi_\theta) := \sum_{t=0}^{T-1} \gamma^t \mathbb{E}_{s_t \sim d_E^t, a_t^E \sim \pi_E, l_t^E \sim \mu_g, \hat{a}_t \sim \pi_\theta} \left[\frac{1}{N_t} (\log \mu_\phi(l_t^E | s_t, a_t^E) - \log \mu_\phi(l_t^E | s_t, \hat{a}_t)) \right], \quad (45)$$

$$\Delta_{r,\phi}(\pi_\theta) \leq N_{\max} \bar{\Delta}_{r,\phi}(\pi_\theta) \quad (46)$$

Then, under Assumption A.7, we can rewrite the

$$\bar{\Delta}_{r,\phi}(\pi_\theta) = \sum_{t=0}^{T-1} \gamma^t \mathbb{E}_{s_t \sim d_t^E, a_t^E \sim \pi_E, l_t^E \sim \mu_g, \hat{a}_t \sim \pi_\theta} \left[\frac{1}{N_t} (\log \mu_\phi(l_t^E | s_t, a_t^E) - \log \mu_\phi(l_t^E | s_t, \hat{a}_t)) \right] \quad (47)$$

$$= \sum_{t=0}^{T-1} q_t p_t \mathbb{E}_{(s_t, a_t, l_t^E) \sim \mathcal{D}_E^{\text{lang}}, \hat{a}_t \sim \pi_\theta(\cdot | s_t)} \left[\frac{1}{N_t} (\log \mu_\phi(l_t^E | s_t, a_t^E) - \log \mu_\phi(l_t^E | s_t, \hat{a}_t)) \right] \quad (48)$$

$$\leq q_{\max} \sum_{t=0}^{T-1} p_t \mathbb{E}_{(s_t, a_t, l_t^E) \sim \mathcal{D}_E^{\text{lang}}, \hat{a}_t \sim \pi_\theta(\cdot | s_t)} \left[\frac{1}{N_t} (\log \mu_\phi(l_t^E | s_t, a_t^E) - \log \mu_\phi(l_t^E | s_t, \hat{a}_t)) \right] \quad (49)$$

$$= q_{\max} (\mathcal{L}_{\text{CE}}(\pi_\theta) - \mathcal{L}_{\text{CE}}(\pi_E)) \quad (50)$$

Also, we have the fact that the clipping has that $x \leq [x]_+$, so we can write:

$$\mathcal{L}_{\text{CE}}(\pi_\theta) - \mathcal{L}_{\text{CE}}(\pi_E) \leq [\mathcal{L}_{\text{CE}}(\pi_\theta) - \mathcal{L}_{\text{CE}}(\pi_E)]_+ = \mathcal{L}_{\text{LC}}(\pi_\theta, \pi_E). \quad (51)$$

Finally, by putting everything together, we have:

$$\Delta_{\text{LC}}(\pi_\theta) \leq \Delta_{r,\phi}(\pi_\theta) + 2\epsilon_\phi \frac{1 - \gamma^T}{1 - \gamma} \quad (52)$$

$$\leq N_{\max} \bar{\Delta}_{r,\phi}(\pi_\theta) + 2\epsilon_\phi \frac{1 - \gamma^T}{1 - \gamma} \quad (53)$$

$$\leq N_{\max} q_{\max} (\mathcal{L}_{\text{CE}}(\pi_\theta) - \mathcal{L}_{\text{CE}}(\pi_E)) + 2\epsilon_\phi \frac{1 - \gamma^T}{1 - \gamma} \quad (54)$$

$$\leq N_{\max} q_{\max} \mathcal{L}_{\text{LC}}(\pi_\theta, \pi_E) + 2\epsilon_\phi \frac{1 - \gamma^T}{1 - \gamma}. \quad (55)$$

Combining Theorem A.4 and Equation (55), we establish the following bound:

Theorem A.8 (LC-loss bounds the performance difference gap). *Combining the result in Equation (55) with Theorem A.4, under Assumptions A.2, A.3 and Assumptions A.5, A.6, A.7, the performance difference gap between the expert policy and the learned policy is bounded by the realized LC-loss up to an LLM-Captioner distillation residual:*

$$|J_{r^*}(\pi_E) - J_{r^*}(\pi_\theta)| \leq w_{\max} \sqrt{\frac{1}{c} \frac{1 - \gamma^T}{1 - \gamma} \left(N_{\max} q_{\max} \mathcal{L}_{\text{LC}}(\pi_\theta, \pi_E) + 2\epsilon_\phi \frac{1 - \gamma^T}{1 - \gamma} \right)}. \quad (56)$$

B Algorithm

The detailed procedures of LC-BC and LC-DP are presented in Algorithm 1 and Algorithm 2, respectively. First, we annotate both the expert dataset \mathcal{D}_E and the general dataset \mathcal{D}_G with language labels by the language label generator μ_g to form $\mathcal{D}_E^{\text{lang}}$ and $\mathcal{D}_G^{\text{lang}}$. Then, the LLM-Captioner μ_ϕ , initialized from a pretrained LLM Ψ and projector weight W , is finetuned from a pretrained LLM on the general dataset $\mathcal{D}_G^{\text{lang}}$ to distill μ_g . In our main results, we use SmoLLM2-135M-Instruct model [92] as the LLM-Captioner’s backbone. Finally, the policy is trained using the proposed LC-loss \mathcal{L}_{LC} computed via the finetuned LLM-Captioner, simultaneously optimizing the original behavior cloning objective \mathcal{L}_{BC} on the expert dataset $\mathcal{D}_E^{\text{lang}}$. This forms the algorithm of language-critique behavior cloning (LC-BC).

For diffusion policies [42], we additionally incorporate a reweighted LC-loss to balance contributions of LC-loss across different diffusion timesteps k , where the reweighting factor is derived in Section E.3. Following Kang et al. [30], we apply one-step reconstruction to recover the clean action from the predicted noise at each timestep, and compute the reweighted LC-loss $\tilde{\mathcal{L}}_{\text{LC}}$ on the reconstructed action \hat{a}_t^0 . The diffusion policy is then optimized jointly with this reweighted LC-loss and the standard diffusion objective \mathcal{L}_{DP} on the expert dataset $\mathcal{D}_E^{\text{lang}}$.

Algorithm 1 Language-critique Behavior Cloning

- 1: **Input:** Expert dataset \mathcal{D}_E , General dataset \mathcal{D}_G , LC-loss weight λ , Feedforward policy π_θ , Language label generator μ_g , and LLM-Captioner μ_ϕ
- 2: Generate $\mathcal{D}_E^{\text{lang}}$ by μ_g with \mathcal{D}_E
- 3: Generate $\mathcal{D}_G^{\text{lang}}$ by μ_g with \mathcal{D}_G
- 4: // Finetune LLM-Captioner μ_ϕ
- 5: Initialize μ_ϕ with a pretrained LLM Ψ and a projector W
- 6: **for** each W finetuning iteration **do**
- 7: Sample $(s_t, a_t, l_t) \sim \mathcal{D}_G^{\text{lang}}$
- 8: Update W with ℓ_{CE}^ϕ from Equation (5)
- 9: **end for**
- 10: **for** each μ_ϕ finetuning iteration **do**
- 11: Sample $(s_t, a_t, l_t) \sim \mathcal{D}_G^{\text{lang}}$
- 12: Update μ_ϕ with ℓ_{CE}^ϕ from Equation (5)
- 13: **end for**
- 14: // Learn policy π_θ
- 15: Randomly initialize π_θ
- 16: **for** each policy iteration **do**
- 17: Sample $(s_t, a_t^E, l_t) \sim \mathcal{D}_E^{\text{lang}}$
- 18: $\hat{a}_t \sim \pi_\theta(\cdot | s_t)$
- 19: Compute \mathcal{L}_{BC} from Equation (10)
- 20: Compute \mathcal{L}_{LC} from Equation (9)
- 21: Update π_θ with $\mathcal{L}_{\text{BC}} + \lambda \mathcal{L}_{\text{LC}}$
- 22: **end for**
- 23: **return** π_θ

Algorithm 2 Language-critique Diffusion Policy

- 1: **Input:** Expert dataset \mathcal{D}_E , General dataset \mathcal{D}_G , LC-loss weight λ , Diffusion policy ϵ_θ , timestep K , Language label generator μ_g , and LLM-Captioner μ_ϕ
- 2: Generate $\mathcal{D}_E^{\text{lang}}$ by μ_g with \mathcal{D}_E
- 3: Generate $\mathcal{D}_G^{\text{lang}}$ by μ_g with \mathcal{D}_G
- 4: // Finetune LLM-Captioner μ_ϕ
- 5: Initialize μ_ϕ with a pretrained LLM Ψ and a projector W
- 6: **for** each W finetuning iteration **do**
- 7: Sample $(s_t, a_t, l_t) \sim \mathcal{D}_G^{\text{lang}}$
- 8: Update W with ℓ_{CE}^ϕ from Equation (5)
- 9: **end for**
- 10: **for** each μ_ϕ finetuning iteration **do**
- 11: Sample $(s_t, a_t, l_t) \sim \mathcal{D}_G^{\text{lang}}$
- 12: Update μ_ϕ with ℓ_{CE}^ϕ from Equation (5)
- 13: **end for**
- 14: // Learn diffusion policy ϵ_θ
- 15: Randomly initialize ϵ_θ
- 16: **for** each policy iteration **do**
- 17: Sample $(s_t, a_t^E, l_t) \sim \mathcal{D}_E^{\text{lang}}$
- 18: Sample $k \sim \text{Uniform}(\{1, \dots, K\})$
- 19: Sample $\epsilon \sim \mathcal{N}(0, \mathbf{I})$
- 20: $a_t^k = \sqrt{\bar{\alpha}^k} a_t^E + \sqrt{1 - \bar{\alpha}^k} \epsilon$
- 21: $\hat{\epsilon} \sim \epsilon_\theta(\cdot | s_t, a_t^k, k)$
- 22: Compute \mathcal{L}_{DP} from Equation (11)
- 23: Reconstruct \hat{a}_t^0 from Equation (12)
- 24: Compute $\tilde{\mathcal{L}}_{\text{LC}}$ with ω^k
- 25: Update ϵ_θ with $\mathcal{L} = \mathcal{L}_{\text{DP}} + \lambda \tilde{\mathcal{L}}_{\text{LC}}$
- 26: **end for**
- 27: **return** ϵ_θ

C Language label details

This section provides additional details on the design and sources of language labels. We first describe the semantic structure of the labels, and then discuss how the language-generation function μ can be instantiated in practice.

Language label design. Assumption A.3 requires that reward-relevant differences in feature space are reflected in the induced language distributions. In other words, when two state-action pairs differ in their reward-relevant semantics, their corresponding language labels should also be distinguishable. This requirement motivates labels that expose task-relevant information rather than unconstrained descriptions of every transition.

Motivated by reward design principles [81, 82], we decompose each language label into three components: task progress <T>, action optimality <A>, and movement guidance <M>. The goal of this decomposition is not to exhaustively describe all aspects of a transition, but to provide structured and compact supervision for learning from mixed-quality demonstrations.

The task-progress component <T> describes the semantic stage of the current state. This component identifies what part of the task has been achieved and which subgoal is currently relevant. For example, in manipulation tasks, <T> may distinguish whether the end-effector is approaching an object, whether the object has been contacted, whether the object is being moved toward the target, or whether the task is completed. By explicitly representing task progress, <T> helps distinguish states

that may be close in raw observation space but correspond to different stages of the long-horizon objective.

The action-optimality component $\langle A \rangle$ characterizes the quality of the demonstrated action under the current task context. Instead of assigning a scalar reward or confidence weight, $\langle A \rangle$ expresses whether the action is beneficial, ineffective, or harmful for task completion. This component is particularly important in mixed-quality datasets, where suboptimal demonstrations may contain both useful intermediate states and undesirable actions. $\langle A \rangle$ provides supervision for deciding which behaviors should be imitated and which should be down-weighted or corrected.

The movement-guidance component $\langle M \rangle$ provides fine-grained corrective information about how the agent should move. While $\langle T \rangle$ captures the high-level task stage and $\langle A \rangle$ captures action quality, $\langle M \rangle$ describes the direction or adjustment needed to make progress. For instance, it may indicate that the agent should move toward a target, align with an object, push in a particular direction, reduce excessive motion, or correct an overshooting behavior. This component is especially useful for continuous-control tasks, where small differences in actions can lead to different outcomes but may not be fully captured by coarse task-stage labels alone.

Together, $\langle T \rangle$, $\langle A \rangle$, and $\langle M \rangle$ provide complementary supervision. $\langle T \rangle$ specifies where the agent is in the task, $\langle A \rangle$ evaluates whether the demonstrated action is appropriate, and $\langle M \rangle$ describes how the behavior should be adjusted. This structured design encourages the induced language distribution to distinguish behaviors that matter for task success while reducing irrelevant variation caused by unconstrained natural language. We evaluate the contribution of these components in Section 5.4.

For example, in the PEGINSERT task (Figure 3e), the robot arm must grasp a peg and insert it into the side of a box. A generated language label may include task progress, such as *Align the peg to the hole.*; action optimality, such as *The action is bad for the state, since the peg misaligns with the hole.*; and movement guidance, such as *Plus, you can pitch to the top softly.* Combined, the final label is: *Align the peg to the hole. But the action is bad for the state, since the peg misaligns with the hole. Plus, you can pitch to the top softly.* Additional examples across tasks are provided in Table 5.

Sources of language labels. Given the desired label structure, the remaining question is how the language-generation function μ is instantiated. In general, μ can take several forms. Human annotators can provide semantically rich feedback, but annotation is labor-intensive, expensive to scale, and may introduce inconsistency. LLMs and VLMs can generate language labels from symbolic states, actions, or visual observations, and have been widely used for language-based reasoning and decision making in embodied agents [93–95]. However, the induced language distribution can vary substantially with the model, prompt template, decoding strategy, and input representation. In addition, LLM-based or VLM-based generation may introduce computational overhead when applied to large offline datasets. Our proposed language label generator provides a controlled alternative: it is less flexible than human or model-generated feedback, but offers reproducible and consistent labels when task states and relevant geometric relations are available.

In this work, we mainly instantiate μ with a language label generator μ_g built on LLF-Bench [33]. We implement a customized version of the LLF-Bench generation pipeline to produce task-specific labels following the $\langle T \rangle$, $\langle A \rangle$, and $\langle M \rangle$ structure described above. This choice allows us to study whether structured language supervision improves offline imitation learning without variation from model sampling, prompt design, or human annotator inconsistency. Although our generator is built on LLF-Bench [33], it differs from the original benchmark in two important ways. First, we propose and implement the structured $\langle T \rangle$, $\langle A \rangle$, and $\langle M \rangle$ decomposition, whereas the original LLF-Bench feedback mainly indicates whether the behavior is good or bad and often contains larger language variations. Our structure is designed to make task progress, action quality, and corrective movement guidance explicit and consistent across the dataset. Second, we extend the generation pipeline beyond the original LLF-Bench domains to cover a broader set of embodied decision-making tasks, including MAZE, BLOCKPUSH, PEGINSERT, and Adroit hand tasks such as HAMMER and RELOCATE. The overall generation details of μ_g are provided in Figure 1.

We additionally evaluate alternative language label sources based on LLM/VLM generation in Section 5.4. Specifically, we collect language labels by prompting `o4-mini`, a multimodal vision-language reasoning model, to generate language labels from trajectory observations. The prompting template is provided in Figure 4, and generated examples are included in Table 5 and Table 6. These

Figure 4: **VLM Prompting.** The prompt we use to generate language labels with o4-mini.

VLM Prompt with o4-mini.

You are shown two images:

- Image 1 is the state BEFORE the action (current state).
- Image 2 is the state AFTER the action (next state).

Below is additional information about the system:

(STATE SPACE) {state space description}

(ACTION SPACE) {action space description}

You are also given the numeric representations of both states and the action taken:

(NUMERIC STATE) current state: {state} ; next state: {next state} ; action taken: {action}

The agent's task is described as follows (in second-person view): {task instruction}

Use BOTH the images and the numeric states to evaluate the transition. Before anything else, identify the main objects in the scene (robot arm, gripper, target object, goal region, obstacles) and reason about their spatial relationships (left/right, nearer/farther, higher/lower, touching/not touching). Use the numeric state values to clarify small or ambiguous visual changes, such as exact distances, object displacement, or contact. Focus on how positions, distances, and contacts changed from the previous state to the next state. Answer the following questions:

1. Using BOTH images and numeric states, describe the relative positions of the agent, the main object, and the goal.
2. In the previous state, determine the agent's task stage based on the gripper-object-goal configuration.
3. Describe the key spatial differences between the two states, focusing ONLY on task-relevant objects such as changes in distance, movement direction, contact, or orientation.
4. Decide whether the action was GOOD or BAD for accomplishing the task goal, tolerating small errors or minor regressions unless the action clearly moves the agent meaningfully farther from success.
5. Provide a concise recommendation for what the agent should do NEXT, specifying clear spatial directions such as move left/right/forward/backward/up/down, open or close the gripper, or push or pull.

First, write a few sentences of reasoning that:

- Describe the relative positions of the agent, the main object, and the goal using both images and numeric states.
- Identify the task stage in the previous state.
- Explain what visually and numerically changed between the two states.
- Justify why the action is good or bad in terms of progress toward the goal.
- Explain why your recommended next movement is appropriate based on spatial reasoning and numeric-state dynamics.

Then, on a NEW LINE at the end, output a single human-style message in the following EXACT format: RESULT: followed by 1-5 short sentences addressed directly to the agent in second person that describe the current task stage, clearly state whether the last action was good or bad, and give a specific spatial recommendation for what to do next.

In the RESULT message:

- Speak directly to the agent using you and your.
- Do NOT mention images, numeric states, coordinates, or technical terms.
- Make it sound like natural human advice rather than a formal report.

You MUST follow the format.

Table 5: **Language label samples.** We listed expert and suboptimal samples for all tasks generated with μ_g .

Task	Expert Samples	Suboptimal Samples
MAZE	You should go in the west direction. Furthermore, the action is good for the state. Plus, you should make a left here.	You should continue in the north direction. Yet, the action is not working for the state. Moreover, you should go slower. Also, you should take a left here.
PARKING	You should now gently park your car into the spot. Moreover, the action is helpful for the state. Furthermore, brake a bit. Also, steer a bit left.	You should first align your car to the parking spot. Even so, the action is not helpful for the state. Plus, slow down a bit. Moreover, steer a bit left.
SWEEP	You should go sideways to the goal. Plus, the action is good for the state. Yet, make a move to the front softly. Plus, please move downward strongly.	You should move to the cube. Yet, the action is bad for the state. Furthermore, the gripper should be opened. Plus, move toward the left firmly.
BOX-CLOSE	You should fetch the lid. Furthermore, the action is useful for the state. Even so, you should move to the front calmly.	You need to raise the lid. Yet, the action is not good for the state. Plus, you should move to the front quickly. Moreover, you need to move to the top quickly.
BLOCKPUSH	Push the second block to the second target. Furthermore, the action is good for the state.	Move to the first block. Plus, the action is bad for the state. Plus, you should move to the front strongly.
PEGINSERT	Insert the peg into the hole. Furthermore, the action is good for the state because the peg is being pushed into the hole. Also, take a move to the bottom gently.	Go to the peg. Yet, the action is not right for the state, since the gripper moves away from the peg. Plus, make a move toward the right gently. Furthermore, make a move to the bottom softly.
HAMMER	You should swing the hammer to the nail. Furthermore, the action is helpful for the state.	You need to move to the hammer. But, the action is not useful for the state. Also, you need to move to the back.
RELOCATE	You need to go to the ball. Furthermore, the action is correct for the state.	You need to move to the ball. Even so, the action is not helpful for the state. Also, you need to move right. Furthermore, you should move toward the front. Plus, you need to reach down.

Table 6: **Language label variant samples.** We listed expert and suboptimal samples for all tasks generated with o4-mini and other variants in Section 5.4.

Task	Expert Samples	Suboptimal Samples
BOX-CLOSE (o4-mini)	You’re in the lift stage and that last move was good. Now move the lid forward and to the right until it’s centered above the box opening.	You’re still trying to grab the lid, and lifting away was a bad move. Lower down and move forward and right to center on the handle. Then close your gripper to secure the lid.
BOX-CLOSE (o4-mini concise)	Lower gripper straight onto handle, open fully and center, clamp down firmly, then lift up.	Maintain the handle alignment, lower gripper, then move forward and close. Last move was unhelpful.
BOX-CLOSE (o4-mini μ_g - style)	You should center the lid. Moreover, the action is good for the state. Yet, lower your gripper straight onto the handle. Also, lift up firmly.	You need to lower the gripper onto the handle and shift forward. However, the action is suboptimal for the state. Moreover, line up before closing the grip.
BOX-CLOSE (μ_g - verbose)	It’s great that you’re trying to retrieve the lid. This action will indeed help with the current situation. Just remember to approach it calmly and smoothly from the front. Keep up the good work!	It seems like you’re trying to get the lid, but at the moment, that action doesn’t seem to be advancing our goal. Let’s adjust our approach here. Instead, move towards the left more decisively, and then slowly inch forward.

experiments allow us to examine whether the proposed framework can benefit from more flexible model-generated language, while the main results use μ_g labels for consistency.

D LLM-Captioner details

In this section, we introduce the model architecture and the detailed training procedure of the LLM-Captioner μ_ϕ . Our objective is to enable end-to-end policy learning to optimize the language-critique imitation objective. To achieve this, the differentiable LLM-Captioner μ_ϕ must distill the language label generator μ_g and provide gradient signals that encourage the policy to match the objective.

The LLM-Captioner μ_ϕ consists of a pretrained transformer backbone Ψ —specifically SmoLM2-135M-Instruct [92]—and an MLP projector W that embeds state–action pairs into the hidden space of the transformer, as illustrated in Figure 5. Further details for the model architecture are provided in Section G.1. The resulting model defines a conditional distribution $\mu_\phi(\cdot | s_t, a_t)$ over language labels, where $\phi = \{\Psi, W\}$ denotes all trainable parameters.

We finetune the LLM-Captioner on the labeled general dataset $\mathcal{D}_G^{\text{lang}}$ using an instruction-tuning pipeline. Training proceeds in two stages: (1) we first update the MLP projector W while keeping the LLM backbone frozen, and (2) we finetune the entire LLM-Captioner μ_ϕ end-to-end, jointly updating both W and Ψ . In both stages, the objective is the cross-entropy loss in Equation (5):

$$\mathbb{E}_{(s_t, a_t, l_t) \sim \mathcal{D}_G^{\text{lang}}} \left[\ell_{\text{CE}}^\phi(l_t, s_t, a_t) \right]$$

The purpose of the finetuned LLM-Captioner μ_ϕ is to distill the generator μ_g for end-to-end policy optimization via gradient descent. Then, the LC-loss constructed by LLM-Captioner encourages

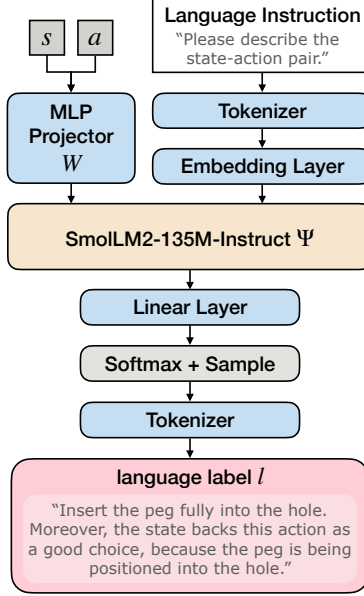


Figure 5: **Model Architecture of LLM-Captioner.** The state-action pair (s, a) is projected into the LLM’s hidden space as a single token via the MLP projector W . This token, concatenated with the language instruction embeddings, serves as input to the decoder transformer Ψ . The final output layer applies a softmax function to sample tokens, generating the resulting language labels l .

the policy to produce actions that align with the expert policy’s behavior with respect to the expert language-critique objective. We ablate backbone choices and finetuning modes in Section I.2.

E LC-DP details

In this section, we provide detailed derivations and implementation details for applying the proposed reweighted LC-loss $\tilde{\mathcal{L}}_{LC}$ to diffusion policies [42] of our method LC-DP. We first review the diffusion model backbone underlying diffusion policies, including the forward diffusion process and the reverse generative process, in Section E.1. Next, we describe the diffusion model training algorithm used for policy learning in Section E.2. Finally, in Section E.3, we derive the timestep-dependent reweighting factor ω^k for LC-DP from the diffusion training algorithm and provide experimental evidence justifying its design.

E.1 Diffusion model: forward and reverse process

We first review the probabilistic formulation of diffusion models, which define paired forward and reverse Markov processes over a sequence of latent variables. As illustrated in Figure 6, diffusion models can be interpreted as latent variable models, where the data distribution over clean samples x^0 is augmented with a sequence of latent variables $\{x^k\}_{k=1}^K$. The joint distribution is defined through a reverse generative process, while the forward process serves as an approximate posterior.

Concretely, in the case of denoising diffusion probabilistic model (DDPM) [96], the forward diffusion process $q(x_{1:K} | x_0)$ is defined as a Markov chain that gradually adds Gaussian noise to the data according to a predefined variance schedule. The forward transitions take the form:

$$q(x^k | x^{k-1}) = \mathcal{N}\left(x^k; \sqrt{\alpha^k}x^{k-1}, (1 - \alpha^k)\mathbf{I}\right), \quad (57)$$

where $\{\alpha^k\}_{k=1}^K$ schedules the noise magnitude at each timestep and $\bar{\alpha}^k = \prod_{i=1}^k \alpha^i$. Due to the linear-Gaussian structure of this process, the latent variable x^k admits a closed-form expression conditioned directly on the clean sample x^0 :

$$x^k = \sqrt{\bar{\alpha}^k}x^0 + \sqrt{1 - \bar{\alpha}^k}\epsilon, \quad \epsilon \sim \mathcal{N}(0, \mathbf{I}). \quad (58)$$

As the timestep k increases, the signal-to-noise ratio decreases and x^k approaches an isotropic Gaussian distribution.

The reverse diffusion process aims to invert the forward diffusion process in order to generatively sample clean data. This is achieved by modeling the conditional distributions $\phi(x^{k-1} | x^k)$, such that samples drawn from the resulting reverse Markov chain approximate the original data distribution. However, directly parameterizing these reverse transitions is generally intractable.

To address this challenge, DDPMs adopt a denoising-based parameterization, in which a neural network is trained to predict the noise injected at each diffusion timestep. Specifically, a model $\epsilon_\theta(x_k, k)$ is optimized to estimate the noise ϵ , allowing recovery of the clean sample from its noisy latent representation. This denoising formulation leads to a simple and stable training objective based on noise prediction, while implicitly defining the reverse generative process.

Diffusion policies [42] adapt the denoising-based diffusion framework to continuous control by modeling a reverse generative process over actions. As illustrated in Figure 7, conditioned on the current state s_t , the diffusion policy samples a clean action \hat{a}_t^0 starting from Gaussian noise $a_t^K \sim \mathcal{N}(0, \mathbf{I})$ and iteratively applying the learned reverse diffusion process. At each diffusion timestep k , the policy predicts the noise component $\hat{\epsilon} \sim \epsilon_\theta(\cdot | s_t, a_t^k, k)$ based on the current state s_t , the intermediate noisy action a_t^k , and the timestep index k , and uses this prediction to produce the next action sample according to the reverse transition:

$$\hat{a}_t^{k-1} = \frac{1}{\sqrt{\alpha^k}} \left(a_t^k - \frac{1 - \alpha^k}{\sqrt{1 - \bar{\alpha}^k}} \epsilon_\theta(\cdot | s_t, a_t^k, k) \right) + \sigma^k z, \quad (59)$$

where $z \sim \mathcal{N}(0, \mathbf{I})$ for $k > 1$ and $z = 0$ for $k = 1$. By iteratively applying this reverse update from $k = K$ to $k = 1$, the diffusion policy progressively denoises the action sample, yielding a clean action \hat{a}_t^0 . This reverse-process formulation implicitly defines a conditional action distribution given the state.

E.2 Diffusion model: training algorithm

Training a diffusion policy reduces to learning a conditional denoising model from expert demonstrations. Given a state-action pair (s_t, a_t^0) sampled from the expert dataset \mathcal{D}_E , where a_t^0 denotes the clean expert action, the training procedure follows the forward–reverse diffusion formulation described in Section E.1.

Specifically, a diffusion timestep k is first sampled uniformly from $\{1, \dots, K\}$. Gaussian noise $\epsilon \sim \mathcal{N}(0, \mathbf{I})$ is then drawn and applied to the clean action a_t^0 according to the forward diffusion process,

$$a_t^k = \sqrt{\bar{\alpha}^k} a_t^0 + \sqrt{1 - \bar{\alpha}^k} \epsilon, \quad (60)$$

where $\bar{\alpha}^k = \prod_{i=1}^k \alpha^i$ denotes the cumulative noise schedule. This operation yields a noisy action a_t^k whose signal-to-noise ratio decreases as the timestep k increases.

The diffusion policy ϵ_θ is trained to predict the injected noise conditioned on the current state, the noisy action, and the diffusion timestep. In practice, the model receives (s_t, a_t^k, k) as input and outputs a noise estimate $\hat{\epsilon} \sim \epsilon_\theta(a_t^k, s_t, k)$. The training objective minimizes the mean squared error

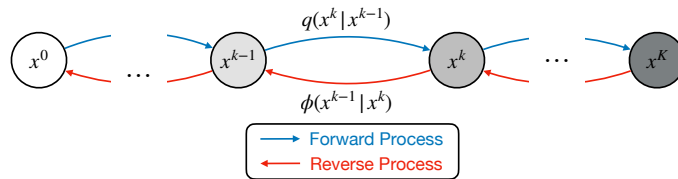


Figure 6: **Illustration of the probabilistic diffusion process.** Latent variables x^1, \dots, x^K are generated from the clean data sample x^0 through a forward diffusion process defined by a probabilistic Markov chain $q(x^k | x^{k-1})$. The reverse process ϕ samples the latent variables from the previous ones to reconstruct the original data sample x^0 via $\phi(x^{k-1} | x^k)$.

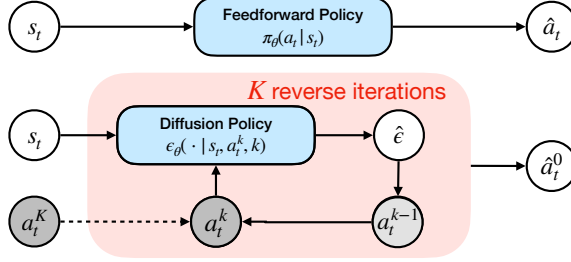


Figure 7: **Action sampling process of a diffusion policy.** Starting from Gaussian noise a_t^K , the diffusion policy iteratively denoises actions conditioned on the current state s_t , producing a clean action sample \hat{a}_t^0 through the learned reverse diffusion process. On the other hand, the feedforward policy predicts an action \hat{a}_t with a single-step inference conditioned on the state.

between the predicted and true noise,

$$\mathcal{L}_{\text{DP}} = \mathbb{E}_{(s_t, a_t^E) \sim \mathcal{D}_E, k, \epsilon \sim \mathcal{N}(0, \mathbf{I})} \left[\left\| \epsilon - \epsilon_\theta(\cdot | s_t, a_t^k, k) \right\|^2 \right]. \quad (61)$$

By training the policy to denoise actions at different noise levels, the model implicitly learns a conditional distribution over clean actions given the state. At inference time, action generation begins from a Gaussian noise sample and iteratively applies the learned reverse process to produce a clean action conditioned on the current state, as illustrated in Figure 7.

E.3 Reweighting factor derivation

To apply language label supervision to diffusion policies, we leverage one-step reconstruction to obtain a clean action estimate from the predicted noise and compute the LC-loss on the reconstructed action. Concretely, although the diffusion policy is trained to predict noise, the predicted noise $\hat{\epsilon} \sim \epsilon_\theta$ can be converted into a reconstructed clean action \hat{a}_t^0 via one-step reconstruction. This allows us to reuse the same LC-loss formulation as in feedforward policies.

A straightforward approach is to directly apply the LC-loss on the reconstructed action without any additional design. However, as shown in Figure 9b, this naive strategy yields limited improvement compared to feedforward policies, suggesting a mismatch between diffusion training dynamics and the action-level supervision induced by the LC-loss.

To better understand this behavior, we analyze the properties of one-step reconstruction across diffusion timesteps. Empirically, we observe that the quality of the reconstructed action \hat{a}_t^0 strongly depends on the diffusion timestep k . Reconstructions from small diffusion steps (small k) are generally accurate, while reconstructions from large diffusion steps (large k) are substantially noisier. This introduces an inherent imbalance: errors from large- k steps dominate the action-level objective, while informative signals from small- k steps are underrepresented.

The standard diffusion policy training objective optimizes noise prediction via the mean squared error

$$\mathcal{L}_{\text{DP}} = \mathbb{E}_{(s_t, a_t^E) \sim \mathcal{D}_E, \epsilon \sim \mathcal{N}(0, \mathbf{I}), k} \left[\left\| \epsilon - \epsilon_\theta(\cdot | s_t, a_t^k, k) \right\|^2 \right] \quad (62)$$

as defined in Equation (11). In contrast, when applying supervision on reconstructed actions, the objective becomes an action-level distance:

$$\mathcal{L}_{\text{DP}}^a = \mathbb{E}_{(s_t, a_t^E) \sim \mathcal{D}_E, \epsilon \sim \mathcal{N}(0, \mathbf{I}), k} \left[\left\| a_t^0 - \hat{a}_t^0 \right\|^2 \right] \quad (63)$$

where \hat{a}_t^0 is obtained via one-step reconstruction in Equation (12). Expanding this action-level objective yields:

$$\|a_t^0 - \hat{a}_t^0\|^2 \quad (64)$$

$$= \left\| a_t^0 - \left(\frac{1}{\sqrt{\bar{\alpha}^k}} a_t^k - \frac{\sqrt{1 - \bar{\alpha}^k}}{\sqrt{\bar{\alpha}^k}} \epsilon_\theta(\cdot | s_t, a_t^k, k) \right) \right\|^2 \quad (65)$$

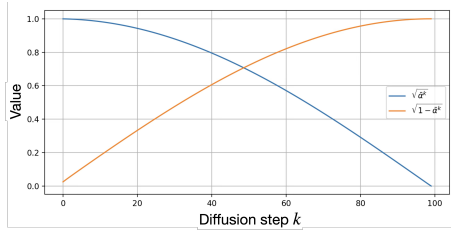
$$= \left\| a_t^0 - \left(\frac{1}{\sqrt{\bar{\alpha}^k}} (\sqrt{\bar{\alpha}^k} a_t^0 + \sqrt{1 - \bar{\alpha}^k} \epsilon) - \frac{\sqrt{1 - \bar{\alpha}^k}}{\sqrt{\bar{\alpha}^k}} \epsilon_\theta(\cdot | s_t, a_t^k, k) \right) \right\|^2 \quad (66)$$

$$= \left\| a_t^0 - \left(a_t^0 + \frac{\sqrt{1 - \bar{\alpha}^k}}{\sqrt{\bar{\alpha}^k}} \epsilon - \frac{\sqrt{1 - \bar{\alpha}^k}}{\sqrt{\bar{\alpha}^k}} \epsilon_\theta(\cdot | s_t, a_t^k, k) \right) \right\|^2 \quad (67)$$

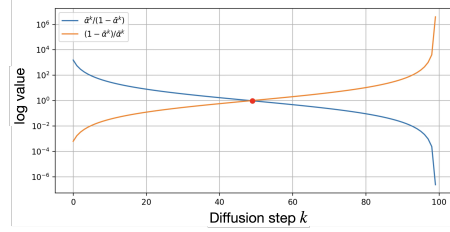
$$= \left\| a_t^0 - a_t^0 + \frac{\sqrt{1 - \bar{\alpha}^k}}{\sqrt{\bar{\alpha}^k}} (\epsilon - \epsilon_\theta(\cdot | s_t, a_t^k, k)) \right\|^2 \quad (68)$$

$$= \frac{1 - \bar{\alpha}^k}{\bar{\alpha}^k} \|\epsilon - \epsilon_\theta(\cdot | s_t, a_t^k, k)\|^2 \quad (69)$$

showing that the action reconstruction error is equivalent to the original noise-prediction error weighted by a timestep-dependent factor $\frac{1 - \bar{\alpha}^k}{\bar{\alpha}^k}$.



(a) Diffusion schedule components over timesteps k : $\sqrt{\bar{\alpha}^k}$ (signal term) and $\sqrt{1 - \bar{\alpha}^k}$ (noise term).



(b) k -dependent weighting induced by one-step reconstruction: $\frac{1 - \bar{\alpha}^k}{\bar{\alpha}^k}$, and its reciprocal reweighting factor ω^k .

Figure 8: **Diffusion schedules and k -dependent reweighting.**

As illustrated in Figure 8, this weighting scheme disproportionately amplifies contributions from large diffusion k -steps at the expense of small- k steps. Directly optimizing this action-level objective introduces unstable training loss convergence; as seen in Figure 9a, the loss exhibits stronger fluctuation, leading to performance degradation. While the resulting policy remains functional, it ultimately underperforms compared to a standard diffusion policy trained with the original noise-prediction loss (Figure 9b).

The above analysis reveals that the action-level objective $\mathcal{L}_{\text{DP}}^a$ implicitly reweights the original diffusion objective \mathcal{L}_{DP} . To recover the balanced training behavior of the standard diffusion loss with one-step reconstructed actions \hat{a}_t^0 , we apply the reciprocal of this k -dependent weight $\frac{1 - \bar{\alpha}^k}{\bar{\alpha}^k}$. Formally, we define the reweighting factor

$$\omega^k := \frac{\bar{\alpha}^k}{1 - \bar{\alpha}^k}. \quad (70)$$

Applying this factor to the action-level objective yields the reweighted action loss

$$\tilde{\mathcal{L}}_{\text{DP}}^a = \mathbb{E}_{(s_t, a_t^E) \sim \mathcal{D}_{E, \epsilon} \sim \mathcal{N}(0, \mathbf{I}), k} \left[\frac{\bar{\alpha}^k}{1 - \bar{\alpha}^k} \|a_t^0 - \hat{a}_t^0\|^2 \right] \quad (71)$$

$$= \mathbb{E}_{(s_t, a_t^E) \sim \mathcal{D}_{E, \epsilon} \sim \mathcal{N}(0, \mathbf{I}), k} \left[\|\epsilon - \epsilon_\theta(\cdot | s_t, a_t^k, k)\|^2 \right] \quad (72)$$

$$= \mathcal{L}_{\text{DP}} \quad (73)$$

showing that the reweighted action objective $\tilde{\mathcal{L}}_{\text{DP}}^a$ is exactly equivalent to the original noise-prediction objective \mathcal{L}_{DP} .

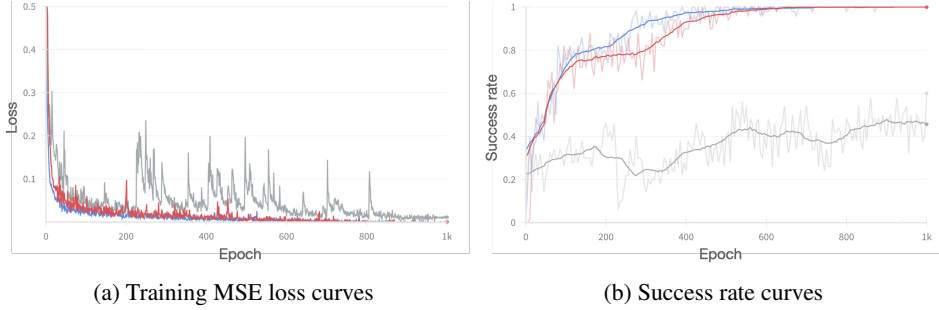


Figure 9: **Diffusion policy training with different objectives.** **Red:** standard noise-prediction loss \mathcal{L}_{DP} ; **gray:** unweighted action-level loss $\mathcal{L}_{\text{DP}}^a$; **blue:** reweighted action-level loss $\tilde{\mathcal{L}}_{\text{DP}}^a$. **Left:** training MSE, where $\mathcal{L}_{\text{DP}}^a$ exhibits large fluctuations due to timestep k imbalance, while the reweighted and original objectives converge stably. **Right:** success rate (evaluated every 5 epochs), showing that reweighting restores near-optimal performance.

We empirically validate this equivalence by training diffusion policies under three objectives: the standard noise-prediction loss \mathcal{L}_{DP} (red), the unweighted action-level loss $\mathcal{L}_{\text{DP}}^a$ (gray), and the reweighted action-level loss $\tilde{\mathcal{L}}_{\text{DP}}^a$ (blue). As shown in Figure 9a and Figure 9b, applying the reweighting factor ω^k aligns both the training loss trajectories and the final performance with those of \mathcal{L}_{DP} , whereas the unweighted action-level objective exhibits noticeable discrepancies. These results confirm the effect and necessity of the proposed reweighting factor ω^k .

With this derivation, we apply the same reweighting factor ω^k to the LC-loss when training diffusion policies. Intuitively, this reweighting compensates for the k -dependent reconstruction bias: without reweighting, inaccuracies at large diffusion steps are overemphasized, while informative gradients from small diffusion steps, where the signal-to-noise ratio is high, are diminished.

This behavior is visualized in Figure 8a and Figure 8b. The original k -dependent weight $\frac{1-\bar{\alpha}^k}{\bar{\alpha}^k}$ (orange curve in Figure 8a) exponentially suppresses contributions from small diffusion steps while amplifying those from large steps. In contrast, its reciprocal ω^k (blue curve in Figure 8a) restores balance by emphasizing small- k steps—where the signal-to-noise ratio is high—and down-weighting large- k steps.

F Environment and tasks details

We list the details of the task environments of Section 5 here. In Table 7, we list the details of expert and general datasets we used for experiments. It comprises the number of trajectories, expert steps, general steps, and the collecting methods. We also provide the environment names, version numbers, the dimensions of state spaces, and action spaces of each task in table 8.

MAZE. A 2D navigation task from [80] in which a point agent learns to navigate from an initial position to a goal position within the medium maze. The 2-DoF agent controls its motion by iteratively applying linear forces along x and y directions. The 6D states include the agent’s two-dimensional current position, velocity, and the goal position. The initial and goal positions of the agent are randomly sampled when an episode is initialized. The maximum episode length for this task is set at 250; termination occurs if the goal is reached earlier.

PARKING. A goal-conditioned continuous control driving task from [84], where the vehicle is asked to park in the designated target spot within a parking lot. The 2-DoF agent navigates the car by controlling the acceleration and steering angle. The 18D observation space includes the current position, the longitudinal velocity, the heading angle of the car, along with the achieved goal state, and the desired target configuration. The dynamics are kinematic bicycle constraints. The maximum episode length for this task is set at 80; termination occurs if the vehicle reaches the target position earlier.

SWEEP. A manipulation task from Metaworld [85] where the agent has to sweep an object off the table. It requires the agent to maintain continuous contact with the object over a long trajectory to the off-table goal. The agent controls the position of the end-effector and the gripper actuation via a 4D continuous action space. The 9D observation states provide the x, y, z position of the robot arm, the manipulation block, and the goal target. The maximum episode length for this task is set at 30, and termination occurs if the object is swept off the table.

BOX-CLOSE. A contact-rich manipulation task from Metaworld [85] in which the agent should grasp the cover and close the box with it. The robot arm should precisely align the position of the cover, grasp the handle, hold it towards the opened box, and put it in a closed position. The agent controls the position of the end-effector and the gripper actuation via a 4D continuous action space. The 9D observation states provide the x, y, z position of the robot arm, the manipulation block, and the target. The maximum episode length for this task is set at 30, and termination occurs if the box is closed with the cover earlier.

BLOCKPUSH. A multistage table-top manipulation task from [47] where a 6-DoF robot arm should push two blocks into two target zones in any order. It is a multimodal task that allows a robot arm to first move one randomly selected block to one target zone, then move the second block to the other zone. The end-effector is controlled via absolute x and y pose on the 2D plane. The 16D observation space encapsulates the full system state, including the current end-effector pose, the position and orientation of both blocks and target zones. The maximum episode length for this task is set at 350, and termination occurs if two blocks are pushed into their corresponding target zones.

PEGINSERT. A high-precision manipulation task from ManiSkill-3 [86] where a 7-DoF robot arm equipped with a gripper must grasp a peg from a table and insert it into a horizontal box hole. This

Table 7: **Dataset.** Detailed information of expert dataset and general dataset in each task.

Task	# of expert trajectories	# of expert steps	# of general steps	Algorithm/Retrieved Sources
MAZE	200	26 037	153 177	D4RL controller [80]
PARKING	500	10 693	73 604	SAC-trained policy expert [97]
SWEEP	500	5035	73 485	Metaworld controller [85]
BOX-CLOSE	500	4214	76 031	Metaworld controller [85]
BLOCKPUSH	500	37 994	301 876	default controller [47]
PEGINSERT	500	18 589	246 576	PPO-trained policy [98]
HAMMER	10	439	24 752	DAPG-trained policy [87]
RELOCATE	20	1118	30 136	DAPG-trained policy [87]

Table 8: **Environments.** Detailed environment setting of each task.

Task	Environment	ID	State space	Action space
MAZE	D4RL [80]	pointmaze-maze2d-medium-v0	6	2
PARKING	Highway-Env [84]	highway-parking-v0	18	2
SWEEP	Metaworld [85]	metaworld-sweep-v2	9	4
BOX-CLOSE	Metaworld [85]	metaworld-box-close-v2	9	4
BLOCKPUSH	BlockPush [47]	blockpushing-BlockPushMultimodal-v0	16	2
PEGINSERT	Maniskill [86]	maniskill-PegInsertionSide-v1	43	8
HAMMER	Gymnasium-Robotics [99]	adroit-hand-hammer-v1	46	26
RELOCATE	Gymnasium-Robotics [99]	adroit-hand-relocate-v1	39	30

task poses accurate control challenges due to the tight clearance between the peg and the hole. The agent operates within a 43D state space, which comprises joint positions and velocities of the robot arm, as well as the poses of both the peg and the target hole. The maximum episode length for this task is set at 100, and termination occurs if the end of the peg is successfully inserted within 0.015m of the center of the box.

HAMMER. A high-dimensional dexterous manipulation task from Gymnasium-Robotics [99] that requires a 28-DoF system, consisting of a 24-DoF ShadowHand and a 4-DoF arm, to pick up a hammer and drive a nail into a board. The environment features a randomized nail position with dry friction capable of absorbing up to 15N of force, requiring the agent to exert significant physical impact. The agent operates within a 26D continuous action space representing the scaled absolute angular positions of the joints, including the arm, wrist, and all finger segments. The 46D observation space tracks joint angles, palm and nail positions, hammer pose and velocities, nail displacement, and impact force. Success is achieved when the entire length of the nail is driven into the board, and the episode is truncated after a maximum of 200 steps.

RELOCATE. A complex manipulation task from Gymnasium-Robotics [99] that utilizes a 30-DoF system, comprising a 24-DoF ShadowHand mounted on a 6-DoF robotic arm. The objective is to pick up a blue ball from a tabletop and move it to a randomly initialized green target in the 3D workspace. The agent utilizes a 30D action space to control arm translation, orientation, and hand joint positions. The 39D observation space tracks joint states and relative 3D vectors between the palm, ball, and target. This task is challenging due to the randomization of both the object and the target, requiring the agent to master a multi-stage behavior: approaching the object, achieving a stable grasp, and precisely transporting the object through free space to an aerial target. The maximum episode length for this task is set at 200, and termination occurs if the blue ball is successfully moved within an epsilon-ball of the target.

G Training details

Our implementation is built on top of the Diffusion Policy codebase [42]. In this section, we describe the model architectures used for all baselines and our proposed methods, along with the corresponding training hyperparameters and computational resources.

G.1 Model architectures

Table 9 and 10 summarize the detailed architectural configurations for all baselines.

Table 9: Model architectures (Part I): MAZE, PARKING, SWEEP, and BOX-CLOSE.

Method	Models	MAZE	PARKING	SWEEP	BOX-CLOSE
BC	Network Type	MLP	MLP	MLP	MLP
	Hidden Dimension	[256, 256, 256, 256]	[256, 256]	[256, 256]	[256, 256]
	Activation Function	tanh	ReLU	ReLU	ReLU
DWBC	Network Type	MLP	MLP	MLP	MLP
	Hidden Dimension	[256, 256, 256, 256]	[256, 256]	[256, 256]	[256, 256]
	Activation Function	tanh	ReLU	ReLU	ReLU
	Discriminator Hidden Dimension	256	256	256	256
DemoDICE	Network Type	MLP	MLP	MLP	MLP
	Hidden Dimension	[256, 256, 256, 256]	[256, 256]	[256, 256]	[256, 256]
	Activation Function	tanh	ReLU	ReLU	ReLU
	Discriminator Network Type	MLP	MLP	MLP	MLP
	Discriminator Hidden Dimension	[256, 256]	[256, 256]	[256, 256]	[256, 256]
	Discriminator Activation Function	ReLU	ReLU	ReLU	ReLU
ILJD	Nu Network Type	MLP	MLP	MLP	MLP
	Nu Hidden Dimension	[256, 256]	[256, 256]	[256, 256]	[256, 256]
	Nu Activation Function	ReLU	ReLU	ReLU	ReLU
LC-BC-reward	R_ϕ Model Type	MLP	MLP	MLP	MLP
	R_ϕ Hidden Dimension	[256, 256, 256]	[256, 256, 256]	[256, 256, 256]	[256, 256, 256]
	R_ϕ Activation Function	ReLU	ReLU	ReLU	ReLU
LC-BC-classifier	C_ϕ Model Type	MLP	MLP	MLP	MLP
	C_ϕ Hidden Dimension	[128, 128]	[256, 256]	[256, 256]	[256, 256]
	C_ϕ Activation Function	ReLU	ReLU	ReLU	ReLU
LC-BC (Ours)	Network Type	MLP	MLP	MLP	MLP
	Hidden Dimension	[256, 256, 256, 256]	[256, 256]	[256, 256]	[256, 256]
	Activation Function	tanh	ReLU	ReLU	ReLU
DP	Network Type	Unet	Unet	Unet	Unet
	Hidden Dimension	[256, 512, 1024]	[256, 512, 1024]	[256, 512, 1024]	[256, 512, 1024]
LPB-Offline	Dynamics Network Type	MLP	MLP	MLP	MLP
	Dynamics Hidden Dimension	[256, 256]	[256, 256]	[256, 256]	[256, 256]
	Dynamics Activation Function	ReLU	ReLU	ReLU	ReLU
EDP	Critic Network Type	MLP	MLP	MLP	MLP
	Critic Hidden Dimension	[256, 256]	[256, 256]	[256, 256]	[256, 256]
	Critic Activation Function	ReLU	ReLU	ReLU	ReLU
LC-DP-reward	Network Type	Unet	Unet	Unet	Unet
	Hidden Dimension	[256, 512, 1024]	[256, 512, 1024]	[256, 512, 1024]	[256, 512, 1024]
	R_ϕ Model Type	MLP	MLP	MLP	MLP
LC-DP-classifier	R_ϕ Hidden Dimension	[64]	[64]	[128, 128]	[128, 128]
	R_ϕ Activation Function	ReLU	ReLU	ReLU	ReLU
	C_ϕ Model Type	MLP	MLP	MLP	MLP
LC-DP (Ours)	C_ϕ Hidden Dimension	[256, 256]	[256, 256]	[256, 256]	[256, 256]
	C_ϕ Activation Function	ReLU	ReLU	ReLU	ReLU
	Network Type	Unet	Unet	Unet	Unet
CQL	Hidden Dimension	[256, 512, 1024]	[256, 512, 1024]	[256, 512, 1024]	[256, 512, 1024]
	Critic Network Type	MLP	MLP	MLP	MLP
	Critic Hidden Dimension	[256, 256]	[256, 256]	[256, 256]	[256, 256]
TD3+BC	Critic Activation Function	ReLU	ReLU	ReLU	ReLU
	Network Type	MLP	MLP	MLP	MLP
	Hidden Dimension	[256, 256, 256, 256]	[256, 256]	[256, 256]	[256, 256]
DT	Activation Function	tanh	ReLU	ReLU	ReLU
	Critic Network Type	MLP	MLP	MLP	MLP
	Critic Hidden Dimension	[256, 256]	[256, 256]	[256, 256]	[256, 256]
	Critic Activation Function	tanh	ReLU	ReLU	ReLU
DT	Transformer	GPT2	GPT2	GPT2	GPT2
	Hidden Size	512	512	512	512
	Number of Layers	6	6	6	6
	Attention Heads	8	8	8	8

Table 10: **Model architectures (Part II): BLOCKPUSH, PEGINSERT, HAMMER, RELOCATE**

Method	Models	BLOCKPUSH	PEGINSERT	HAMMER	RELOCATE
BC	Network Type	Unet	MLP	MLP	MLP
	Hidden Dimension	[256, 512, 1024]	[256, 256]	[256, 256]	[256, 256]
	Activation Function	-	tanh	ReLU	ReLU
DWBC	Network Type	Unet	MLP	MLP	MLP
	Hidden Dimension	[256, 512, 1024]	[256, 256]	[256, 256]	[256, 256]
	Activation Function	-	tanh	ReLU	ReLU
	Discriminator Hidden Dimension	256	256	256	256
DemoDICE	Network Type	Unet	MLP	MLP	MLP
	Hidden Dimension	[256, 512, 1024]	[256, 256]	[256, 256]	[256, 256]
	Activation Function	-	tanh	ReLU	ReLU
	Discriminator Network Type	MLP	MLP	MLP	MLP
	Discriminator Hidden Dimension	[128, 128]	[256, 256]	[256, 256]	[256, 256]
Nu	Network Type	MLP	MLP	MLP	MLP
	Hidden Dimension	[128, 128]	[256, 256]	[256, 256]	[256, 256]
	Activation Function	ReLU	ReLU	ReLU	ReLU
ILID	Network Type	Unet	MLP	MLP	MLP
	Hidden Dimension	[256, 512, 1024]	[256, 256]	[256, 256]	[256, 256]
	Activation Function	-	tanh	ReLU	ReLU
	Discriminator Network Type	MLP	MLP	MLP	MLP
	Discriminator Hidden Dimension	[256]	[256]	[256]	[256]
LC-BC-reward	R_ϕ Model Type	MLP	MLP	MLP	MLP
	R_ϕ Hidden Dimension	[256, 256]	[256, 256]	[128]	[128]
	R_ϕ Activation Function	ReLU	ReLU	ReLU	ReLU
LC-BC-classifier	Network Type	Unet	MLP	MLP	MLP
	Hidden Dimension	[256, 512, 1024]	[256, 256]	[256, 256]	[256, 256]
	Activation Function	-	tanh	ReLU	ReLU
LC-BC-classifier	C_ϕ Model Type	MLP	MLP	MLP	MLP
	C_ϕ Hidden Dimension	[128]	[256, 256]	[256]	[256]
	C_ϕ Activation Function	ReLU	ReLU	ReLU	ReLU
LC-BC (Ours)	Network Type	Unet	MLP	MLP	MLP
	Hidden Dimension	[256, 512, 1024]	[256, 256]	[256, 256]	[256, 256]
	Activation Function	-	tanh	ReLU	ReLU
DP	Network Type	Unet	Unet	Unet	Unet
	Hidden Dimension	[256, 512, 1024]	[256, 512, 1024]	[256, 512, 1024]	[256, 512, 1024]
LPB-Offline	Dynamics Network Type	MLP	MLP	MLP	MLP
	Dynamics Hidden Dimension	[256, 256]	[256, 256]	[256, 256]	[256, 256]
	Dynamics Activation Function	ReLU	ReLU	ReLU	ReLU
EDP	Critic Network Type	Unet	MLP	MLP	MLP
	Critic Hidden Dimension	[256, 256]	[256, 256]	[256, 256]	[256, 256]
	Critic Activation Function	ReLU	ReLU	ReLU	ReLU
LC-DP-reward	Network Type	Unet	Unet	Unet	Unet
	Hidden Dimension	[256, 512, 1024]	[256, 512, 1024]	[256, 512, 1024]	[256, 512, 1024]
	Activation Function	-	tanh	ReLU	ReLU
LC-DP-classifier	C_ϕ Model Type	MLP	MLP	MLP	MLP
	C_ϕ Hidden Dimension	[128]	[256, 256]	[128]	[128]
	C_ϕ Activation Function	ReLU	ReLU	ReLU	ReLU
LC-DP (Ours)	Network Type	Unet	Unet	Unet	Unet
	Hidden Dimension	[256, 512, 1024]	[256, 512, 1024]	[256, 512, 1024]	[256, 512, 1024]
	Activation Function	-	tanh	ReLU	ReLU
CQL	Critic Network Type	MLP	MLP	MLP	MLP
	Critic Hidden Dimension	[256, 256]	[256, 256]	[256, 256]	[256, 256]
	Critic Activation Function	ReLU	ReLU	ReLU	ReLU
TD3+BC	Network Type	Unet	MLP	MLP	MLP
	Hidden Dimension	[256, 512, 1024]	[256, 256]	[256, 256]	[256, 256]
	Activation Function	-	tanh	ReLU	ReLU
DT	Transformer	GPT2	GPT2	GPT2	GPT2
	Hidden Size	1024	512	128	128
	Number of Layers	6	6	2	4
DT	Attention Heads	8	8	4	4

G.2 Hyperparameters

Table 11 lists the training hyperparameters used for all baselines and our proposed methods. Unless otherwise specified, we set the gradient accumulation step to 1. For LC-BC and LC-DP, we explicitly increase the gradient accumulation steps to accommodate the additional memory cost introduced by LLM-based computations, allowing us to use smaller per-step batch sizes within our computational constraints.

Table 11: **Hyperparameters.** The overview of the hyperparameters used for all the methods in every task. We abbreviate "Gradient Accumulation" as "Grad Acc." and "Finetune" as "FT" in this table.

Method	Hyperparameter	MAZE	PARKING	SWEEP	BOX-CLOSE	BLOCKPUSH	PEGINSERT	HAMMER	RELOCATE
BC	Policy Batch Size	128	128	128	128	256	128	128	128
	Policy Learning Rate	1e-4	1e-4	1e-2	1e-2	2e-4	1e-3	1e-3	1e-3
	Policy Epochs	1001	1001	1001	1001	1001	1001	1001	1001
DWBC	Policy Batch Size	128	128	128	128	256	128	128	128
	Policy Learning Rate	1e-4	3e-4	3e-4	3e-4	2e-4	1e-4	3e-4	3e-5
	α	7.5	10	7.5	7.5	15	12	7.5	10
	Discriminator Hidden Dim. logpi	128	128	128	128	128	128	128	128
	Discriminator Hidden Dim. sa	128	128	128	128	128	128	128	128
	Policy Epochs	1001	1001	1001	1001	401	401	1001	1001
DemoDICE	Policy Batch Size	128	128	128	128	256	128	128	128
	Policy Learning Rate	1e-4	3e-4	1e-4	5e-4	1e-4	1e-3	1e-4	5e-5
	α	0.1	0.1	0.1	0.05	0.01	0.1	0.1	0.1
	Policy Epochs	1001	1001	1001	1001	1001	401	1001	1001
ILID	Policy Batch Size	128	128	128	128	256	128	128	128
	Policy Learning Rate	1e-4	1e-4	1e-2	1e-2	2e-4	1e-3	1e-3	1e-3
	Discriminator Learning Rate	1e-4	1e-4	1e-4	1e-4	1e-4	1e-4	1e-4	1e-4
	Rollback steps	5	3	3	5	5	3	5	3
	Rollback Decay Rate	0.9	0.9	0.9	0.9	0.9	0.9	0.9	0.9
	Select Threshold	0.89	0.89	0.89	0.89	0.89	0.89	0.89	0.89
LC-BC-reward	Reward Model Batch Size	256	256	256	256	512	512	256	256
	Reward Model Learning Rate	1e-4	1e-4	1e-4	1e-4	1e-4	1e-4	1e-4	1e-4
	Reward Model Epochs	2001	2000	1001	1001	501	501	200	500
	Policy Batch Size	128	128	128	128	256	128	128	128
	Policy Reward Loss Weight	1e-2	1e-2	1e-3	1e-3	1e-4	1e-2	1e-2	1e-2
LC-BC-classifier	Policy Learning Rate	1e-4	1e-4	1e-2	1e-2	2e-4	1e-3	1e-3	1e-3
	Policy Epochs	1001	1001	1001	1001	1001	1001	1001	1001
	Classifier Model Batch Size	256	256	256	256	512	256	256	256
	Classifier Model Learning Rate	1e-4	1e-4	1e-4	1e-4	5e-5	1e-4	1e-4	1e-4
	Classifier Model Epochs	1000	1000	1000	1000	1000	1000	1000	1000
	Classifier Heads	6	7	6	6	4	10	7	6
	Classifier Classes	8	3	3	3	4	11	4	3
	Policy Batch Size	128	128	128	128	256	128	128	128
	Policy Class Loss Weight	1e-4	1e-4	1e-4	1e-4	2e-4	1e-4	1e-1	1e-4
	Policy Learning Rate	1e-4	1e-2	1e-2	1e-2	1e-3	1e-3	1e-2	1e-3
LC-BC (Ours)	Policy Epochs	1001	1001	1001	1001	1001	1001	1001	1001
	MLP Projector Batch Size	128	128	128	128	128	64	128	128
	MLP Projector Grad Acc.	4	2	2	2	4	8	2	2
	MLP Projector Learning Rate	1e-4	1e-4	1e-4	1e-4	1e-4	1e-4	1e-4	1e-4
	MLP Projector Epochs	100	100	100	100	100	100	100	100
	μ_ϕ FT Batch Size	128	128	128	128	128	64	128	128
	μ_ϕ FT Grad Acc.	1	1	1	1	1	2	1	1
	LLM-Captioner FT Learning Rate	1e-5	5e-5	5e-5	1e-4	1e-5	1e-5	1e-4	1e-4
	MLP Projector FT Learning Rate	1e-5	5e-5	5e-5	1e-4	1e-5	1e-5	5e-5	5e-5
	μ_ϕ FT Epochs	10	10	10	10	10	10	10	10
DP	Policy Batch Size	16	16	16	16	16	16	32	16
	Policy Grad Acc.	8	8	8	8	16	8	4	8
	LC-loss Weight	1e-2	1e-2	1e-2	1e-2	1e-4	1e-2	1e-2	1e-2
	Policy Learning Rate	1e-4	1e-4	1e-2	1e-2	2e-4	1e-3	1e-3	1e-3
	Policy Epochs	1001	1001	1001	1001	1001	1001	1001	1001
	Policy Epochs	1001	1001	1001	1001	1001	1001	1001	1001
LPB	Policy Batch Size	256	256	256	256	256	256	256	256
	Policy Learning Rate	1e-4	1e-4	1e-4	1e-4	1e-4	1e-5	1e-4	1e-4
	Policy Epochs	1001	1001	1001	1001	1001	1001	1001	1001
EDP	Dynamic model Batch Size	256	256	256	256	256	256	256	256
	Dynamic model Learning Rate	1e-4	1e-4	1e-4	1e-4	1e-4	1e-5	1e-4	1e-4
	Dynamic model Epochs	1001	1001	1001	1001	1001	1001	1001	1001
	Pretrain Policy Batch Size	256	256	256	256	256	256	256	256
	Pretrain Policy Alpha	1e-2	1e-2	1e-3	1e-3	1e-3	1e-3	1e-3	1e-3
EDP	Pretrain Policy Learning Rate	1e-4	1e-4	1e-4	1e-4	1e-5	1e-4	1e-4	1e-4
	Pretrain Policy Epochs	1001	1001	1001	1001	501	1001	1001	1001
	Policy Batch Size	256	256	256	256	256	256	256	256
	Policy Alpha	1e-2	1e-2	1e-3	1e-3	1e-3	1e-3	1e-3	1e-3
	Policy Learning Rate	1e-4	1e-4	1e-4	1e-4	1e-4	1e-4	1e-4	1e-4
Policy Epochs	1001	1001	1001	1001	1001	1001	1001	1001	

Table 11: Hyperparameters (Continued)

Method	Hyperparameter	MAZE	PARKING	SWEEP	BOX-CLOSE	BLOCKPUSH	PEGINSERT	HAMMER	RELOCATE
LC-DP-reward	Reward Model Batch Size	256	256	256	256	256	512	256	256
	Reward Model Learning Rate	1e-6	1e-5	1e-5	1e-5	1e-6	1e-6	1e-4	1e-4
	Reward Model Epochs	1000	1000	500	500	100	500	200	500
	Policy Batch Size	256	256	256	256	256	256	256	256
	Policy Reward Loss Weight	1e-3	1e-3	1e-2	1e-3	1e-4	1e-3	1e-2	1e2
	Policy Learning Rate	1e-4	1e-4	1e-4	1e-4	1e-4	1e-4	1e-4	1e-4
LC-DP-classifier	Policy Epochs	1001	1001	1001	1001	1001	1001	1001	1001
	Classifier Model Batch Size	256	256	256	256	512	256	256	256
	Classifier Model Learning Rate	1e-4	1e-4	1e-4	1e-4	1e-5	1e-4	1e-4	1e-4
	Classifier Model Epochs	1000	1000	1000	1001	1000	1000	1000	1000
	Classifier Heads	6	7	6	6	4	10	7	6
	Classifier Classes	8	3	3	3	4	11	4	3
LC-DP (Ours)	Policy Batch Size	256	256	256	256	256	256	256	256
	Policy Class Loss Weight	1e-4	1e-3	1e-4	1e-4	1e-3	1e-4	1e-4	1e-3
	Policy Learning Rate	1e-4	1e-4	1e-4	1e-4	1e-4	1e-4	1e-4	1e-4
	Policy Epochs	1001	1001	1001	1001	1001	1001	1001	1001
	MLP Projector Batch Size	128	128	128	128	128	64	128	128
	MLP Projector Grad Acc.	4	2	2	2	4	8	2	2
LC-DP (Ours)	MLP Projector Learning Rate	1e-4	1e-4	1e-4	1e-4	1e-4	1e-4	1e-4	1e-4
	MLP Projector Epochs	100	100	100	100	100	100	100	100
	μ_ϕ FT Batch Size	128	128	128	128	128	64	128	128
	μ_ϕ FT Grad Acc.	1	1	1	1	1	2	1	1
	LLM-Captioner FT Learning Rate	1e-5	5e-5	5e-5	5e-5	1e-5	1e-5	1e-4	1e-4
	MLP Projector FT Learning Rate	1e-5	5e-5	5e-5	5e-5	1e-5	1e-5	5e-5	5e-5
CQL	μ_ϕ FT Epochs	10	10	10	10	10	10	10	10
	Policy Batch Size	16	16	16	16	16	16	16	16
	Policy Grad Acc.	16	16	16	16	16	16	16	16
	LC-loss Weight	1e-2	1e-4	1e-3	1e-4	1e-5	1e-2	5e-2	1e-3
	Policy Learning Rate	1e-4	1e-4	1e-4	1e-4	1e-4	1e-4	1e-4	1e-4
	Policy Epochs	1001	1001	1001	1001	1001	1001	1001	1001
CQL	Policy Batch Size	128	128	128	128	256	128	128	128
	Critic Learning Rate	3e-4	1e-4	1e-4	1e-4	1e-4	1e-5	1e-4	1e-4
	Policy Learning Rate	1e-4	1e-4	1e-4	1e-4	1e-4	1e-4	1e-4	1e-4
	Policy Epochs	3001	3001	1001	2001	1001	1001	1001	1001
	BC Training Epochs	1000	200	200	200	1000	200	200	200
	CQL α'	5.0	10.0	5.0	10.0	10.0	5.0	5.0	5.0
TD3+BC	CQL action samples	64	64	64	64	64	32	64	64
	Pretrain Batch Size	128	128	128	128	256	128	128	128
	Pretrain Alpha	1e-3	1e-4	1e-3	1e-3	1e-3	1e-3	1e-3	1e-3
	Pretrain Learning Rate	1e-4	1e-4	1e-3	1e-3	1e-5	1e-4	1e-3	1e-3
	Pretrain Epochs	1001	1001	1001	1001	1001	1001	1001	1001
	FT Batch Size	128	128	128	128	256	128	128	128
DT	FT Alpha	1e-3	1e-4	1e-3	1e-3	1e-3	1e-3	1e-3	1e-3
	FT Learning Rate	1e-3	1e-4	1e-3	1e-3	2e-4	1e-3	1e-3	1e-3
	FT Epochs	1001	1001	1001	1001	1001	1001	1001	1001
	Policy Batch Size	256	256	256	256	256	256	256	256
	Policy Learning Rate	1e-4	1e-4	1e-4	1e-4	1e-4	1e-4	5e-5	5e-5
	Policy Epochs	1001	1001	1001	1001	1001	1001	1001	1001
	Target Return	100.45082	18.32615	6.21332	5.72269	36.94823	22.09803	29.38271	27.49282

G.3 Computational resources

Table 12 reports the computational resources we have used for our experiments, including the workstation configurations.

Table 12: Computation resources.

Workstation	CPU	GPU	RAM
1	Intel Xeon W-2255	NVIDIA GeForce RTX 3090, NVIDIA GeForce RTX 3080	125G
2	Intel Xeon W-2255	NVIDIA GeForce RTX 3090, NVIDIA GeForce RTX 3080	125G
3	Intel Xeon W-2255	NVIDIA GeForce RTX 3080 Ti \times 2	125G
4	Intel Xeon W-2255	NVIDIA GeForce RTX 4070 Ti \times 2	125G
5	Intel Xeon W-2255	NVIDIA GeForce RTX 4070 Ti \times 2	125G
6	Intel Xeon W-2255	NVIDIA GeForce RTX 4070 Ti \times 2	125G
7	Intel Xeon W-2255	NVIDIA GeForce RTX 4070 Ti \times 2	125G
8	Intel Xeon W-2255	NVIDIA GeForce RTX 4070 Ti \times 2	125G
9	Intel Xeon w7-2475X	NVIDIA GeForce RTX 4090 \times 2	125G
10	Intel Xeon w7-2475X	NVIDIA GeForce RTX 4090 \times 2	125G
11	Intel Xeon w5-2455X	NVIDIA RTX A6000 \times 2	125G
12	Intel Xeon Platinum 8480+	NVIDIA H100 \times 2	500G

H Baseline details

H.1 LC-BC-reward and LC-DP-reward

We design two reward-based ablation baselines, LC-BC-reward and LC-DP-reward, as scalar-reward counterparts to LC-BC and LC-DP, respectively. These baselines test whether the gains of language-critique imitation arise merely from learning an auxiliary scalar reward model, or from preserving the structured information contained in language label supervision. Both baselines follow the same overall pipeline as our language-based methods: first, a reward predictor is trained on the general dataset; second, the reward predictor is frozen and used to provide auxiliary supervision during policy learning on the expert dataset. Thus, LC-BC-reward and LC-DP-reward replace the language model μ_ϕ and the LC-loss with a scalar reward model R_ϕ and a reward-critique loss.

Reward model. Given a reward-labeled general dataset $\mathcal{D}_G^r = \{(s_t, a_t, r_t)\}$, we train a reward model R_ϕ to predict the scalar reward associated with each state-action pair. The reward model is optimized with a mean squared error objective:

$$\mathcal{L}_R^\phi = \mathbb{E}_{(s_t, a_t, r_t) \sim \mathcal{D}_G^r} \left[\|R_\phi(s_t, a_t) - r_t\|_2^2 \right]. \quad (74)$$

After training, R_ϕ is frozen and used for downstream policy optimization.

Reward-critique loss. Given the frozen reward model R_ϕ , we define a reward-based analogue of the LC-loss on the expert dataset $\mathcal{D}_E^r = \{(s_t, a_t^E, r_t)\}$. For a policy action $\hat{a}_t \sim \pi_\theta(\cdot | s_t)$, we define the policy reward-prediction loss and the expert reward-prediction loss as

$$\mathcal{L}_R(\pi_\theta) = \mathbb{E}_{(s_t, r_t) \sim \mathcal{D}_E^r, \hat{a}_t \sim \pi_\theta(\cdot | s_t)} \left[\|R_\phi(s_t, \hat{a}_t) - r_t\|_2^2 \right], \quad (75)$$

$$\mathcal{L}_R(\pi_E) = \mathbb{E}_{(s_t, a_t^E, r_t) \sim \mathcal{D}_E^r} \left[\|R_\phi(s_t, a_t^E) - r_t\|_2^2 \right]. \quad (76)$$

The reward-critique loss clips the policy loss at the expert loss:

$$\mathcal{L}_{RC}(\pi_\theta, \pi_E) = [\mathcal{L}_R(\pi_\theta) - \text{sg}(\mathcal{L}_R(\pi_E))]_+, \quad (77)$$

where $[x]_+ = \max(x, 0)$ and $\text{sg}(\cdot)$ denotes stop-gradient. This objective penalizes policy actions whose predicted rewards are less consistent with the expert reward labels than the corresponding expert actions, and the penalty vanishes once the policy matches the expert under the frozen reward model.

Reward-critique behavior cloning. LC-BC-reward applies the reward-critique loss to a feedforward behavior cloning policy. The standard behavior cloning objective is

$$\mathcal{L}_{BC} = \mathbb{E}_{(s_t, a_t^E) \sim \mathcal{D}_E, \hat{a}_t \sim \pi_\theta(\cdot | s_t)} \left[\|a_t^E - \hat{a}_t\|_2^2 \right]. \quad (78)$$

LC-BC-reward jointly optimizes the imitation loss and the reward-critique loss:

$$\mathcal{L}_{BC} + \lambda \mathcal{L}_{RC}(\pi_\theta, \pi_E), \quad (79)$$

where λ controls the strength of reward guidance.

Reward-critique diffusion policy. LC-DP-reward applies the same reward-critique principle to diffusion policy. The diffusion policy ϵ_θ is trained with the standard noise-prediction objective

$$\mathcal{L}_{DP} = \mathbb{E}_{(s_t, a_t^E) \sim \mathcal{D}_E, \epsilon \sim \mathcal{N}(0, \mathbf{I}), k} \left[\|\epsilon - \hat{\epsilon}\|_2^2 \right], \quad \hat{\epsilon} \sim \epsilon_\theta(\cdot | s_t, a_t^k, k). \quad (80)$$

Since the diffusion policy predicts noise rather than actions, we apply the reward-critique loss to the one-step reconstructed action

$$\hat{a}_t^0 = \frac{1}{\sqrt{\bar{\alpha}^k}} a_t^k - \frac{\sqrt{1 - \bar{\alpha}^k}}{\sqrt{\bar{\alpha}^k}} \hat{\epsilon}, \quad \hat{\epsilon} \sim \epsilon_\theta(\cdot | s_t, a_t^k, k). \quad (81)$$

Following Section E.3, we use the timestep-dependent weight $\omega^k = \frac{\bar{\alpha}^k}{1-\bar{\alpha}^k}$ to reduce the imbalance caused by noisier reconstructions at larger diffusion steps. The reweighted reward-prediction losses are

$$\tilde{\mathcal{L}}_R(\pi_\theta) = \mathbb{E}_{(s_t, r_t) \sim \mathcal{D}_E^r, \hat{a}_t^0 \sim \epsilon_\theta(s_t), k} \left[\omega^k \|R_\phi(s_t, \hat{a}_t^0) - r_t\|_2^2 \right], \quad (82)$$

$$\tilde{\mathcal{L}}_R(\pi_E) = \mathbb{E}_{(s_t, a_t^E, r_t) \sim \mathcal{D}_E^r, k} \left[\omega^k \|R_\phi(s_t, a_t^E) - r_t\|_2^2 \right]. \quad (83)$$

The reweighted reward-critique loss is then

$$\tilde{\mathcal{L}}_{RC}(\pi_\theta, \pi_E) = \left[\tilde{\mathcal{L}}_R(\pi_\theta) - \text{sg} \left(\tilde{\mathcal{L}}_R(\pi_E) \right) \right]_+. \quad (84)$$

The final LC-DP-reward objective is

$$\mathcal{L}_{DP} + \lambda \tilde{\mathcal{L}}_{RC}(\pi_\theta, \pi_E). \quad (85)$$

LC-DP-reward therefore trains the diffusion policy to predict noise such that the reconstructed actions both remain close to expert actions and match the expert scalar rewards under the frozen reward model. Unlike LC-DP, however, LC-DP-reward compresses behavioral supervision into scalar rewards and therefore cannot preserve the structured behavioral distinctions provided by language label.

H.2 LC-BC-classifier and LC-DP-classifier

We design two multi-head categorical baselines, LC-BC-classifier and LC-DP-classifier, as discrete-classification variants to LC-BC and LC-DP, respectively. These baselines convert each language label l_t into a tuple of categorical indices $c_t = (c_t^T, c_t^A, c_t^M)$ corresponding to the task progress <T>, action optimality <A>, and movement guidance <M>, discarding the natural-language form.

We test whether the gains of language-critique imitation arise from the expressiveness of natural language and the capacity of a pretrained language model to capture inter-label dependencies, or the independent categorical predictions over the same label dimensions. Both baselines follow the same two-stage pipeline: first, a multi-head classifier is trained on the general dataset with categorical labels c_t ; second, the classifier is frozen and used for auxiliary supervision during policy learning on the expert dataset. Thus, LC-BC-classifier and LC-DP-classifier replace the language model μ_ϕ and the LC-loss with a multi-head classifier C_ϕ and a classifier-critique loss.

Classifier model. Each language label is decomposed into H independent categorical dimensions corresponding to task progress <T>, action optimality <A>, and movement guidance <M>, with C_h classes for each dimension $h \in \{1, \dots, H\}$. Given a categorically labeled general dataset $\mathcal{D}_G^c = \{(s_t, a_t, c_t)\}$, where $c_t = (c_t^1, \dots, c_t^H) \in \{1, \dots, C_1\} \times \dots \times \{1, \dots, C_H\}$ encodes the class index for each dimension, we train a multi-head classifier C_ϕ that maps each state-action pair to per-head logits. The classifier consists of a shared MLP encoder followed by H parallel linear heads, where head h outputs logits $C_\phi^h(s_t, a_t) \in \mathbb{R}^{C_h}$. The classifier is optimized with a cross-entropy objective averaged over heads:

$$\mathcal{L}_C^\phi = \mathbb{E}_{(s_t, a_t, c_t) \sim \mathcal{D}_G^c} \left[\frac{1}{H} \sum_{h=1}^H \text{CE}(C_\phi^h(s_t, a_t), c_t^h) \right], \quad (86)$$

where $\text{CE}(\cdot, \cdot)$ denotes the standard cross-entropy loss. After training, C_ϕ is frozen and used for downstream policy optimization.

Classifier-critique loss. Given the frozen classifier C_ϕ , we define a classification-based analogue of the LC-loss on the expert dataset $\mathcal{D}_E^c = \{(s_t, a_t^E, c_t)\}$. For a policy action $\hat{a}_t \sim \pi_\theta(\cdot | s_t)$, the policy classification loss and the expert classification loss are

$$\mathcal{L}_C(\pi_\theta) = \mathbb{E}_{(s_t, c_t) \sim \mathcal{D}_E^c, \hat{a}_t \sim \pi_\theta(\cdot | s_t)} \left[\frac{1}{H} \sum_{h=1}^H \text{CE}(C_\phi^h(s_t, \hat{a}_t), c_t^h) \right], \quad (87)$$

$$\mathcal{L}_C(\pi_E) = \mathbb{E}_{(s_t, a_t^E, c_t) \sim \mathcal{D}_E^c} \left[\frac{1}{H} \sum_{h=1}^H \text{CE}(C_\phi^h(s_t, a_t^E), c_t^h) \right]. \quad (88)$$

The classifier-critique loss clips the policy loss at the expert loss:

$$\mathcal{L}_{CC}(\pi_\theta, \pi_E) = [\mathcal{L}_C(\pi_\theta) - \text{sg}(\mathcal{L}_C(\pi_E))]_+. \quad (89)$$

This objective penalizes policy actions whose predicted class distributions are less consistent with the expert categorical labels than the corresponding expert actions.

Classifier-critique behavior cloning. LC-BC-classifier jointly optimizes the behavior cloning loss (Equation (78)) and the classifier-critique loss:

$$\mathcal{L}_{BC} + \lambda \mathcal{L}_{CC}(\pi_\theta, \pi_E), \quad (90)$$

where λ controls the strength of classifier guidance.

Classifier-critique diffusion policy. LC-DP-classifier applies the classifier-critique principle to diffusion policy. As in LC-DP-reward, the classifier-critique loss is applied to the one-step reconstructed action \hat{a}_t^0 (Equation (81)). Following Section E.3, we use the timestep-dependent weight $\omega^k = \frac{\bar{\alpha}^k}{1 - \bar{\alpha}^k}$. The reweighted classification losses are

$$\tilde{\mathcal{L}}_C(\pi_\theta) = \mathbb{E}_{(s_t, c_t) \sim \mathcal{D}_E^c, \hat{a}_t^0 \sim \epsilon_\theta(s_t), k} \left[\frac{\omega^k}{H} \sum_{h=1}^H \text{CE}(C_\phi^h(s_t, \hat{a}_t^0), c_t^h) \right], \quad (91)$$

$$\tilde{\mathcal{L}}_C(\pi_E) = \mathbb{E}_{(s_t, a_t^E, c_t) \sim \mathcal{D}_E^c, k} \left[\frac{\omega^k}{H} \sum_{h=1}^H \text{CE}(C_\phi^h(s_t, a_t^E), c_t^h) \right]. \quad (92)$$

The reweighted classifier-critique loss is then

$$\tilde{\mathcal{L}}_{CC}(\pi_\theta, \pi_E) = [\tilde{\mathcal{L}}_C(\pi_\theta) - \text{sg}(\tilde{\mathcal{L}}_C(\pi_E))]_+. \quad (93)$$

The final LC-DP-classifier objective is

$$\mathcal{L}_{DP} + \lambda \tilde{\mathcal{L}}_{CC}(\pi_\theta, \pi_E). \quad (94)$$

Comparison with LC-BC/LC-DP. LC-BC-classifier and LC-DP-classifier preserve the same structured label dimensions as language label ($\langle T \rangle$, $\langle A \rangle$, $\langle M \rangle$) but discard two properties of language-based supervision: (i) the inter-label dependencies captured by the autoregressive pretrained language model, and (ii) the grounding of categorical distinctions in natural-language semantics through pretrained token embeddings. By reducing language labels to independent categorical predictions, these baselines isolate whether the structured label dimensions alone drive the gains, or whether the expressiveness of natural language supervision is essential.

I Additional experimental results

I.1 VLM-generated language labels.

In Table 3, we study whether general-purpose VLMs can serve as an alternative to our proposed language generator μ_g on the task BOX-CLOSE. Specifically, we replace the generator μ_g in Section 4.2 with o4-mini prompting, using the template in Figure 4. However, directly using o4-mini-generated language labels with the small SmoLLM2-135M-Instruct LLM-Captioner yields limited gains: LC-BC reaches only 55.2%, which is comparable to shuffled μ_g labels (55.6%), and LC-DP reaches 63.6%. This suggests that open-ended VLM labels are not automatically useful for language-critique imitation. One possible reason is that VLM labels are often verbose, diverse, and redundant, which makes their distribution harder for μ_ϕ to model and may introduce noisy supervision during policy training.

We therefore evaluate two ways to improve VLM-based supervision. First, we increase the capacity of μ_ϕ from SmoLLM2-135M-Instruct to SmoLLM2-360M-Instruct, testing whether a stronger captioner can better model the more diverse o4-mini label distribution. This improves both methods, with LC-BC increasing from 55.2% to 61.6% and LC-DP increasing from 63.6% to 71.2%, even surpassing the μ_g result for LC-DP. Second, we post-process o4-mini labels to reduce linguistic redundancy. Asking an LLM to make the labels concise improves LC-BC to 63.4% but does not improve LC-DP. In contrast, using an LLM to rewrite o4-mini labels into a μ_g -style structured format performs worse, reaching only 56.4% for LC-BC and 62.4% for LC-DP. This indicates that surface-level structure or style alone is insufficient.

To understand this failure, we compare o4-mini labels against μ_g labels by treating μ_g as a feature-aligned reference. The match rates are low: o4-mini agrees with μ_g on only 51.8% of <T> descriptions, 46.1% of <A> descriptions, and 18.8% of <M> descriptions. Specifically, accuracy is particularly low for fine-grained movement guidance (18.8% for <M> labels) compared to higher-level task progress (51.8% for <T>). This suggests that current VLMs struggle with the precise spatial reasoning required to describe state-action effects in continuous control. Overall, these results suggest that the degraded performance of VLM-generated labels comes from two sources: linguistic verbosity and semantic inaccuracy. The latter is especially severe for fine-grained movement guidance, where accurate <M> labels require precise spatial reasoning over state-action effects. We further isolate the effects of linguistic form versus semantic content using two controlled μ_g variants:

- μ_g -shuffled: Preserves the concise, structured form but destroys semantic alignment.
- μ_g -verbose: Preserves semantic correctness but rewrites labels into diverse, verbose, and human-like language.

The μ_g -shuffled baseline preserves concise and structured label form but destroys semantic accuracy, while the μ_g -verbose variant preserves semantic correctness but rewrites labels into more diverse, verbose, and human-like language. For LC-BC, μ_g -verbose substantially improves over shuffled labels (68.0% vs. 55.6%), suggesting that semantic accuracy is more important than concise surface form for feedforward policies. Although μ_g -verbose still underperforms the original concise μ_g labels (80.4%), it remains clearly beneficial when the label content is accurate. For LC-DP, however, μ_g -verbose does not improve over shuffled labels and remains below the best o4-mini result with the larger LLM-Captioner. This suggests that diffusion-policy training is more sensitive to label distribution complexity and benefits more from concise or well-modeled language supervision. This is aligned with the observations from o4-mini-generated labels plus the larger LLM-Captioner backbone SmoLLM2-360M-Instruct.

Overall, VLM-generated language labels can be useful when paired with a stronger LLM-Captioner, but μ_g remains the most reliable source of supervision because it provides both semantic consistency and feature-aligned structure to exploit useful behaviors to optimize policy from expert and suboptimal demonstrations.

I.2 LLM-Captioner ablation

Table 13 ablates the choice of LLM-Captioner backbone and the degree to which it is finetuned. We vary the backbone across SmoLLM2-135M-Instruct [92], SmoLLM2-360M-Instruct [92],

Table 13: **LLM-Captioner ablation.** We ablate the choice of LLM-Captioner backbone and finetuning strategy, reporting mean and standard deviation across 50 environment rollouts and 5 seeds for both LC-BC and LC-DP on the task BOX-CLOSE. (% omitted.)

Backbone	Finetune mode	LC-BC	LC-DP
SmoLLM2-135M-Instruct	Full-model	80.4 \pm 4.6	69.2 \pm 6.7
SmoLLM2-135M-Instruct	Projector-only	62.0 \pm 14.3	66.4 \pm 7.1
SmoLLM2-135M-Instruct	Pretrained	53.6 \pm 8.2	60.0 \pm 15.0
SmoLLM2-360M-Instruct	Full-model	55.2 \pm 6.6	66.0 \pm 4.9
Qwen2-0.5B-Instruct	Full-model	67.2 \pm 17.1	62.4 \pm 6.1
Mistral-7B-Instruct-v0.3	Projector-only	61.2 \pm 7.9	58.8 \pm 5.4

Qwen2-0.5B-Instruct [100], and Mistral-7B-Instruct-v0.3 [101], and consider three finetuning regimes: full-model finetuning, projector-only finetuning (with the LLM-Captioner backbone frozen), and a pretrained baseline that uses the LLM-Captioner off-the-shelf without any task-specific adaptation. Please refer to Section D for architectural details.

First, adaptation matters far more than scale: the smallest backbone, SmoLLM2-135M-Instruct, achieves the best LC-BC score 80.4% when fully finetuned, and degrades substantially when only the projector is trained 62.0% or when the pretrained model is used 53.6%. Projector-only training on the much larger Mistral-7B-Instruct-v0.3 (61.2%) does not recover this gap, suggesting that simply increasing parameter count without exposing the language model to the task is insufficient.

Second, scaling the backbone under full-model finetuning does not yield consistent gains—SmoLLM2-360M-Instruct 55.2% and Qwen2-0.5B-Instruct 67.2% both underperform the 135M variant and exhibit higher variance across seeds. Results on LC-DP are noisier and show a smaller spread across configurations, but the same qualitative ordering holds, with full finetuning of the 135M backbone remaining competitive. We therefore adopt SmoLLM2-135M-Instruct with full-model finetuning as our default LLM-Captioner: it is the smallest, fastest option and also the most accurate, indicating that the captioner’s backbone is not the main bottleneck for our methods.

I.3 LLM-Captioner training data analysis

Our framework uses the general dataset \mathcal{D}_G and the expert dataset \mathcal{D}_E , following the typical problem setup of imitation learning from suboptimal demonstrations. The policy is trained on \mathcal{D}_E (with the standard BC or diffusion objective on expert actions and the LC-loss evaluated on expert language labels), while the LLM-Captioner is fine-tuned on the full $\mathcal{D}_G^{\text{lang}}$. Since the policy training objective does not directly consume suboptimal trajectories, it is important to verify that the general dataset provides a meaningful contribution through the LLM-Captioner. To this end, we train an expert-only captioner μ_ϕ^E on $\mathcal{D}_E^{\text{lang}}$ alone and use it for downstream LC-BC and LC-DP training. Table 14 reports results on BOX-CLOSE over 50 environment rollouts and 5 training seeds.

Table 14: **LLM-Captioner training data analysis.** We compare LLM-Captioner training on the full general dataset \mathcal{D}_G against training on the expert subset \mathcal{D}_E only, evaluated on BOX-CLOSE over 50 rollouts and 5 seeds (% omitted). Removing \mathcal{D}_G from captioner training degrades LC-BC by 21.2% and LC-DP by 13.2%, driving LC-DP below the plain DP baseline.

Method	μ_ϕ training data	BOX-CLOSE
BC	–	54.8 \pm 8.4
LC-BC	\mathcal{D}_E only	59.2 \pm 10.4
LC-BC	\mathcal{D}_G (ours)	80.4 \pm 4.6
DP	–	64.8 \pm 5.0
LC-DP	\mathcal{D}_E only	56.0 \pm 9.1
LC-DP	\mathcal{D}_G (ours)	69.2 \pm 6.7

Removing \mathcal{D}_G from captioner training degrades LC-BC from 80.4% to 59.2%—recovering only 4.4% over plain BC (54.8%). For LC-DP, the effect is more severe: the expert-only captioner drops

performance to 56.0%, below the plain DP baseline (64.8%), indicating that a captioner without contrastive supervision can actively harm policy learning.

When μ_ϕ is trained on the full $\mathcal{D}_G^{\text{lang}}$, it observes both expert and suboptimal behaviors paired with their structured labels and learns a discriminative mapping that distinguishes good from bad behaviors. The LC-loss then transmits this discrimination to the policy at expert states. When μ_ϕ is trained only on $\mathcal{D}_E^{\text{lang}}$, it never observes negative or corrective labels, so its likelihood landscape over language labels becomes unable to distinguish action quality. The resulting LC-loss provides weak, non-discriminative gradients for LC-BC and noisy gradients that destabilize diffusion training for LC-DP. These results confirm that the general dataset is essential despite never entering the policy objective directly. \mathcal{D}_G provides the contrastive supervision that shapes μ_ϕ , which in turn transmits behavioral-quality distinctions to the policy via the LC-loss. Without it, the framework collapses toward standard expert-only imitation.

I.4 λ sensitivity

We study the effect of the coefficient λ , which balances the behavior cloning (BC) objective and the LC-loss for LC-BC, and the diffusion objective and the LC-loss for LC-DP. In Figure 10, we evaluate $\lambda \in \{1.0, 0.1, 0.01, 0.001, 0.0001\}$. The results show that feedforward policies improve consistently by a large margin, but are sensitive to larger values of λ , with $\lambda \geq 1.0$ leading to degraded performance, whereas diffusion policies improve over $\lambda \in \{1.0, 0.1, 0.0001\}$, but degrade at moderate λ .

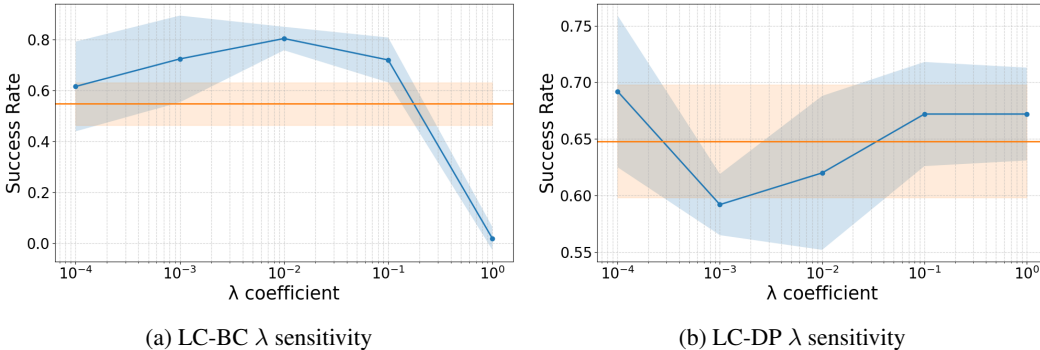


Figure 10: λ **sensitivity**. Blue curves represent LC-BC and LC-DP, while orange horizontal lines represent BC and DP performance. We vary the balancing coefficient $\lambda \in \{1.0, 0.1, 0.01, 0.001, 0.0001\}$.

J Qualitative results of LC-loss and LLM-Captioner

To evaluate the qualitative performance, we visualize the execution of PEGINSERT and BOX-CLOSE tasks. We display six key frames for each, accompanied by the instantaneous LC-loss and the generated language labels. The results demonstrate that LC-BC achieves significantly lower LC-loss compared to BC due to the direct optimization of this objective. This stability allows LC-BC to generate language labels that offer clear, corrective semantic guidance even when the agent faces potential misalignment. This capability to detect and correct errors via language ensures robust performance and task success.

In the PEGINSERT task (Figure 11), the LC-BC agent successfully aligns and inserts the peg and maintains a perfect LC-loss of 0.0. The generated language labels provide accurate, actionable corrections, and generate precise instructions like, "Yet the action is not good for the state, as the peg misaligns with the hole. Also, you should yaw toward the left softly." allowing it to identify the misalignment of the peg and the hole and include accurate correction, which leads to the success of the task. In contrast, the BC policy achieves a relatively low LC-loss, but the peg remains outside the hole; when the observation deviates from the desired state, the policy fails to recover.

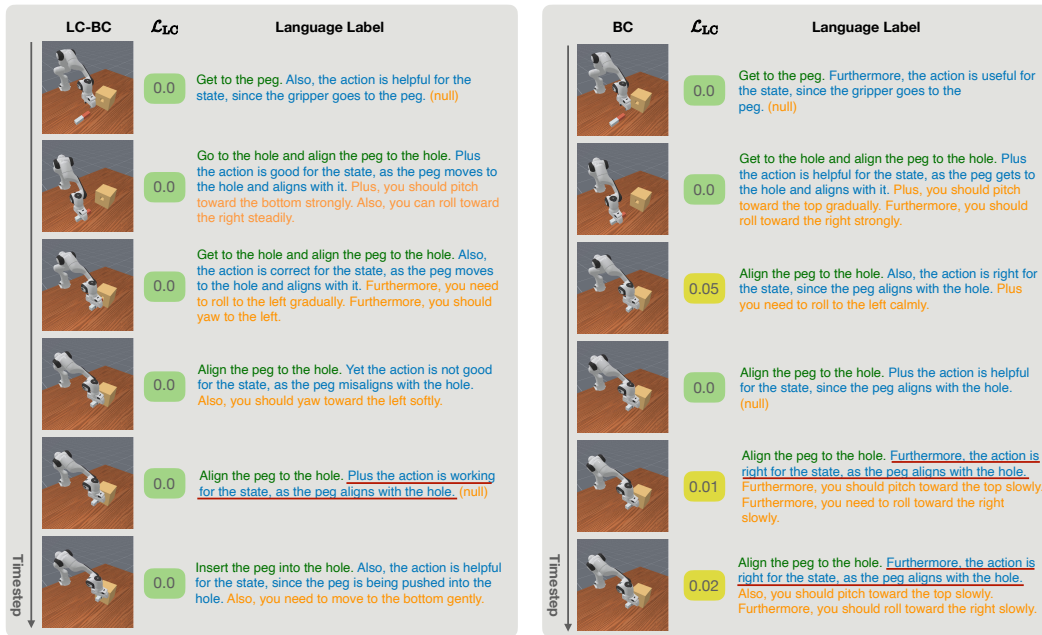


Figure 11: Qualitative result of PEGINSERT.

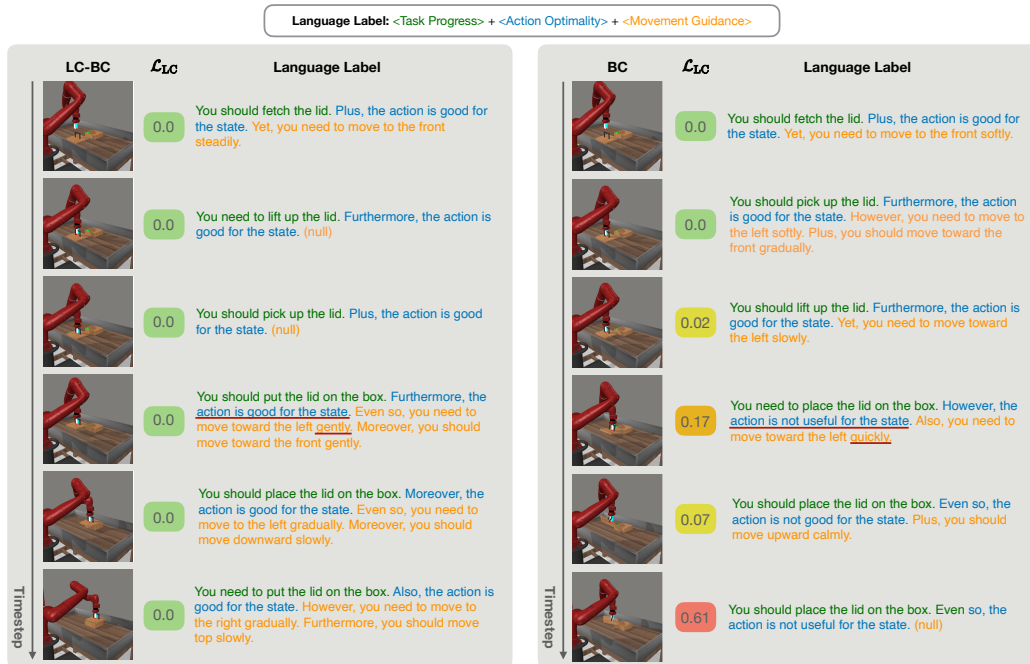


Figure 12: Qualitative result of BOX-CLOSE.

For BOX-CLOSE task (Figure 12), the LC-BC agent maintains a consistently low LC-loss throughout the episode; this stability is reflected in the generated language labels. From the fourth key frame of LC-BC, it shows that instructions like *"the action is good for the state."* and *"you need to move toward the left gently"* provide assessment of action and movement guidance. As a result, the LC-BC agent successfully aligns the lid and closes the box. On the other hand, the BC agent struggles as the task progresses, its LC-loss spikes significantly (reaching 0.17 and 0.61) in the later stages, and the BC agent cannot recover from errors once the observation drifts from the training distribution, thus resulting in failure of the task.

K Impact statement

This work studies the use of natural-language feedback as a supervision signal for offline imitation learning in continuous-control settings. By providing structured guidance, our approach improves learning from suboptimal datasets. Our approach directly advances the potential applications of continuous-control systems, with promising applications in robotic control. We do not foresee immediate negative societal impacts beyond these considerations.

L Limitations

While our proposed framework demonstrates strong performance on continuous-control benchmarks, it has several limitations. The language feedback used as supervision may reflect implicit biases derived from its source, and structured language critiques are most naturally suited to tasks with semantically interpretable motions; for tasks such as locomotion, where behavioral distinctions are difficult to articulate in natural language, language labels may be less informative. Additionally, the two-stage pipeline introduces computational overhead relative to standard behavior cloning, as training and evaluating the language model μ_ϕ adds cost despite being frozen during policy learning.

Our current label generator μ_g relies on designed heuristics over privileged state information; replacing it with a vision-language model would broaden applicability to image-based settings, but existing VLMs do not yet produce the fine-grained, action-level critiques our framework requires, making this a promising direction for future work. More broadly, our empirical evaluations are restricted to offline continuous-control benchmarks, and it remains an open question how well the approach generalizes to more complex and dynamic real-world robotic settings.